Westinghouse Non-Proprietary Class 3

WCAP-16083-NP
Revision 1

April 2013

Benchmark Testing of the FERRET Code for Least Squares Evaluation of Light Water Reactor Dosimetry

WCAP-16083-NP
Revision 1

Benchmark Testing of the FERRET Code for Least Squares Evaluation of Light Water Reactor Dosimetry

Greg A. Fischer*
Radiation Engineering & Analysis

April 2013

Reviewer: Joel A. Kulesza*
Radiation Engineering & Analysis

Approved: Laurent P. Houssay*, Manager
Radiation Engineering & Analysis

*Electronically approved records are authenticated in the electronic document management system.

Westinghouse Electric Company LLC
1000 Westinghouse Drive
Cranberry Township, PA 16066, USA

RECORD OF REVISIONS

Rev.	Date	Revision Description
0	May 2004	Original issue (WCAP-16083-NP)
0	May 2006	Approved version issued (WCAP-16083-NP-A)
1	See EDMS	Appendices A and B have been added to discuss RAPTOR-M3G and BUGLE-B7. Minor editorial modifications have been made, and the references have been updated to reflect the latest versions of WCAP documents and ASTM standards.

TABLE OF CONTENTS

LIST OF TABLES

LIST OF FIGURES

1 INTRODUCTION

To assess embrittlement of Light Water Reactor (LWR) pressure vessels, accurately evaluating the neutron exposure of the materials comprising the beltline region of the vessel is required. This exposure evaluation must, in general, include assessments not only at locations of maximum exposure at the inner diameter of the vessel, but also as a function of axial, azimuthal, and radial location throughout the vessel wall.

To satisfy the requirements of 10CFR50, Appendices G and H[1] for calculating pressure/temperature limit curves for normal reactor coolant system heatup and cooldown, fast neutron exposure levels must be defined at depths within the vessel wall equal to 25% and 75% of the wall thickness for each of the materials comprising the beltline region. These locations are commonly referred to as the 1/4T and 3/4T positions in the vessel wall. The 1/4T exposure levels are also used in the determination of upper shelf fracture toughness as specified in 10CFR50, Appendix G. To determine the pressurized thermal shock reference temperature (RT_{PTS}) for comparison with the applicable screening criteria as defined in 10CFR50.61[2], maximum neutron exposure levels experienced by each of the beltline materials are required. These maximum levels occur at the vessel inner radius. Furthermore, if performing a probabilistic fracture mechanics analysis of the pressure vessel, a complete neutron exposure profile is required for the entire pressure vessel beltline volume.

Methods acceptable to the NRC staff for determining the neutron exposure of LWR pressure vessels are described in Regulatory Guide 1.190, "Calculational and Dosimetry Methods for Determining Pressure Vessel Neutron Fluence."[3] This Regulatory Guide requires the exposure projections to be completed with a calculation. It also requires that measurements be used to qualify the calculational methodology, to identify biases in the calculations, and to provide reliable estimates of the uncertainties in the exposure projections. The guide also states that, in the determination of potential biases and uncertainties, measurement to calculation (M/C) comparisons should include a suitably weighted average of individual M/C values that accounts for the spectral coverage of the sensor set and the uncertainties in the measurements, the dosimetry cross-sections, and the neutron energy spectrum.

The methodology described in this report is based on applying benchmarked, plant-specific neutron transport calculations providing neutron exposure maps throughout the reactor geometry including the pressure vessel wall, all in-vessel, and/or ex-vessel measurement locations. Evaluating the dosimetry from the in-vessel and/or ex-vessel irradiations is subsequently accomplished with a least squares analysis. This includes both the calculation and measurement data to establish best estimates of exposure parameters with reduced uncertainties at the measurement locations. The least squares evaluations results are used to demonstrate consistency among the various measurements and the baseline calculation at all measurement points and to validate the calculated results within the pressure vessel wall.

A least squares adjustment method to perform dosimetry evaluations represents a rigorous approach to weighting the spectral coverage of individual sensor measurements and to combining the uncertainties associated with the transport calculations, measured reaction rates, and dosimetry cross-sections. Further, the results of the least squares evaluations provide comparisons of the best estimates of exposure parameters of interest (Fluence [E > 1.0 MeV] and iron atom displacements [dpa]) with the corresponding calculated results before adjustment. It is these damage exposure parameters and their uncertainties rather than individual sensor reaction rates that are of the ultimate interest.

This approach is summarized in ASTM E944, "Standard Guide for Application of Neutron Spectrum Adjustment Methods in Reactor Surveillance,"[4] which states the following:

> "Adjustment methods provide a means for combining the results of neutron transport calculations with neutron dosimetry measurements in order to obtain optimal estimates for neutron damage exposure parameters with assigned uncertainties. The inclusion of measurements reduces the uncertainties for these parameter values and provides a test for the consistency between measurements and calculations and between different measurements."

The least squares adjustments described in this report are used to combine multiple foil sensor measurements and plant-specific calculated neutron spectra to determine best estimate exposure parameters only at in-vessel and ex-vessel measurement locations. This approach allows for appropriate spectral weighting of the measurements obtained from the multiple foil sensor sets. It also provides a rigorous treatment of the various measurement and calculational uncertainties associated with the process. Thus, the application of the least squares procedure allows the validation of the transport calculations to be based on comparisons of the exposure parameters of interest such as ϕ (E > 1.0 MeV) rather than on some combination of individual sensor M/C ratios.

In this application, the FERRET code[5,6] is used for the least squares analysis of the dosimetry data sets. That is, the FERRET code is used solely to determine the best estimate exposure at locations where calculations and measurements coincide. The relationship between the best estimate exposure at the measurement locations and that at the pressure vessel wall, where no measurements exist, is not addressed internal to the FERRET code. Rather, the results of the plant-specific neutron transport calculations are relied on to relate the neutron exposure at the pressure vessel wall to that at the various measurement locations within the reactor downcomer and/or the ex-vessel cavity. This is analogous to an approach where one might use spatial calculations throughout the reactor core in addition to measurements at the center of selected fuel assemblies to generate detailed core power distribution maps that include locations removed from the measurement positions.

This is in contrast to the more sophisticated LEPRICON code system[7], which performs simultaneous adjustments of the calculated neutron spectra at the various measurement locations and at the pressure vessel wall in order to determine the best estimate exposure with associated uncertainties within the pressure vessel itself.

The purpose of this report is to describe the application of the FERRET code to the least squares analysis of typical LWR dosimetry sets irradiated at either in-vessel or ex-vessel locations and to summarize the testing of the FERRET approach in both benchmark and power reactor neutron fields. The results provided in this report are intended to validate the FERRET code and the least squares procedure for use in the analysis of LWR dosimetry.

2 DESCRIPTION OF THE LEAST SQUARES METHODOLOGY

2.1 BACKGROUND

Least squares adjustment methods provide the capability to combine measurement data with the results of neutron transport calculations to establish a best estimate neutron energy spectrum with associated uncertainties at the measurement locations. Best estimates for key exposure parameters such as neutron flux, ϕ (E > 1.0 MeV), or iron atom displacement rate, dpa/s, along with their uncertainties are then easily obtained from the adjusted spectrum. Using measurements in combination with detailed transport calculations results in a reduced uncertainty in the calculated spectrum, and provides a method to identify any biases or inconsistencies that may exist in the baseline transport calculation or in the measured data.

The application of least squares adjustment methods in LWR dosimetry analysis is common throughout the dosimetry community. The American Society for Testing and Materials (ASTM) has addressed the use of adjustment codes in ASTM E944 "Application of Neutron Spectrum Adjustment Methods in Reactor Surveillance," and many industry workshops have been held to discuss the various applications. For example, the ASTM-EURATOM Symposia on Reactor Dosimetry holds workshops on neutron spectrum unfolding and adjustment techniques at each of its bi-annual conferences.

In ASTM E944, a comprehensive listing of available adjustment codes commonly employed in reactor surveillance programs including STAY'SL[8], LSL-M2[9], FERRET, and LEPRICON is provided. Each of these codes is publicly available from the Radiation Safety Information Computational Center (RSICC) at the Oak Ridge National Laboratory (ORNL).

The FERRET code was initially developed at the Hanford Engineering Development Laboratory (HEDL) and has had extensive use in both the Liquid Metal Fast Breeder (LMFBR) program and the NRC sponsored Light Water Reactor Surveillance Dosimetry Improvement Program (LWR-PV-SDIP). Examples of prior use of the FERRET code for LWR applications include: 1) a re-evaluation of the dosimetry from commercial pressurized water reactor surveillance capsules[12] and 2) an evaluation of the dosimetry included in the PCA blind test experiments[13]. Both of these applications were completed in support of the LWR-PV-SDIP program.

The former evaluation was carried out to establish an updated surveillance capsule dosimetry database for use in the establishment of improved trend curves defining the radiation induced shift in reference nil ductility transition temperature and the decrease in upper shelf energy versus neutron fluence or displacements per atom (dpa). These updated correlations were later used in the development of the trend curve data appearing in Regulatory Guide 1.99, Revision 2[14, 15, 16, 17]. The latter evaluation was completed to provide estimates of key exposure parameters (Fluence E > 1.0 MeV and dpa) for use in performing blind tests of neutron transport calculations in the PCA facility[12, 13]. This allowed blind test comparisons of calculated exposure parameters directly with the least squares results. It also allowed comparisons with measured reaction rates obtained from the multiple foil sensor sets included in the PCA irradiations.

By participating in several cooperative efforts associated with the LWR-PV-SDIP, the FERRET approach was adopted by Westinghouse in the mid 1980s as the preferred approach to evaluating LWR surveillance dosimetry. The least squares methodology was judged to be superior to the previously employed spectrum averaged cross-section approach, which is dependent on the accuracy of the shape of the calculated

neutron spectrum at the measurement locations. Further, applying the least squares methodology allowed for a rigorous treatment of the uncertainties associated with the dosimetry evaluation process.

2.2 APPLICATION OF THE METHODOLOGY

In general, the least squares methods, as applied to LWR dosimetry evaluations, act to reconcile the measured sensor reaction rate data, dosimetry reaction cross-sections, and the calculated neutron energy spectrum within their respective uncertainties. For example,

$$R_i \pm \delta_{R_i} = \sum_g (\sigma_{ig} \pm \delta_{\sigma_{ig}})(\phi_g \pm \delta_{\phi_g})$$

relates a set of measured reaction rates, R_i, to a single neutron spectrum, ϕ_g, through the multigroup dosimeter reaction cross-section, σ_{ig}, each with an uncertainty δ. The primary objective of the least squares evaluation is to produce unbiased estimates of the neutron exposure parameters at the location of the measurement.

The application of the least squares methodology requires the following input:

1. The calculated neutron energy spectrum and associated uncertainties at the measurement location.

2. The measured reaction rates and associated uncertainty for each sensor contained in the multiple foil set.

3. The energy-dependent dosimetry reaction cross-sections and associated uncertainties for each sensor contained in the multiple foil sensor set.

For LWR dosimetry applications, the calculated neutron spectrum is obtained from the results of plant-specific neutron transport calculations that follow the guidelines specified in Regulatory Guide 1.190[3].

The sensor reaction rates are derived from the measured specific activities obtained using established ASTM procedures. The dosimetry reaction cross-sections and uncertainties are obtained from the SNLRML dosimetry cross-section library. Each of these critical input parameters and associated uncertainties are discussed in this section.

2.3 NEUTRON TRANSPORT CALCULATIONS AND UNCERTAINTIES

An accurate plant-specific neutron transport solution with its associated uncertainty represents the foundation upon which the least squares analysis of in-vessel and ex-vessel dosimetry sets builds. Therefore, in this section, the methodology employed by Westinghouse to perform neutron and gamma ray transport calculations for LWR applications is described in some detail. Also included is a discussion of the benchmarking of the analysis approach and the resultant uncertainties associated with the calculational results.

For most routine analyses, the calculation of the neutron and gamma ray environment within the reactor geometry is completed on a fuel cycle-specific basis using the following three-dimensional flux synthesis technique:

$$\phi(r,\theta,z) = [\phi(r,\theta)] * [\phi(r,z)]/[\phi(r)]$$

where $\phi(r,\theta,z)$ is the synthesized three-dimensional neutron flux distribution, $\phi(r,\theta)$ is the transport solution in r,θ geometry, $\phi(r,z)$ is the two-dimensional solution for a cylindrical reactor model using the actual axial core power distribution, and $\phi(r)$ is the one dimensional solution for a cylindrical reactor model using the same source per unit height as that used in the r,θ two dimensional calculation.

All of the transport calculations are carried out using the DORT discrete ordinates code Version 3.1[10] and the BUGLE-96 cross-section library[11]. The BUGLE-96 library provides a 67 group coupled neutron-gamma ray cross-section data set produced specifically for light water reactor application. Anisotropic scattering is treated with a minimum P_3 legendre expansion and the angular discretization is modeled with a minimum S_8 order of angular quadrature. Energy- and space-dependent core power distributions as well as system operating temperatures are treated on a fuel cycle-specific basis. The synthesis procedure combining the $\phi(r,\theta)$, $\phi(r,z)$, and $\phi(r)$ transport solutions into the three-dimensional flux/fluence maps within the reactor geometry is accomplished via post-processing of the scalar flux files generated as a part of the DORT output.

In some extreme cases in which three-dimensional effects reduce the accuracy of the synthesis approach, a fully three-dimensional analytical approach may be used to perform the transport analysis. In these instances, the TORT[10] three-dimensional discrete ordinates code, included as a part of the DOORS 3.1 code package, may be used in either x,y,z or r,θ,z geometry to effect the three-dimensional solution. As in the case of the transport calculations used in the synthesis analysis, the TORT calculations use the BUGLE-96 cross-section library with a minimum P_3 scattering approximation and a minimum S_8 order of angular quadrature.

More information regarding updated neutron transport software is available in Appendix A.

2.3.1 Geometric Modeling

In developing an analytical model of the LWR reactor geometry, nominal design dimensions are normally employed for the various structural components. In some cases, as-built dimensions are available; in those instances, the more accurate as-built data are used for model development. However, most as-built dimensions of the components in the beltline region of the reactor are not available; instead, design dimensions are used. Likewise, water temperatures and, hence, coolant density in the reactor core and downcomer regions of the reactor are normally taken to be representative of full power operating conditions. The reactor core is treated as a homogeneous mixture of fuel, cladding, water, and miscellaneous core structures such as fuel assembly grids, guide tubes, etc. Sensitivities of the analytical results to tolerances in the internals dimensions and fluctuations in water temperature are discussed and quantified in Section 2.3.4.

The r,θ geometric mesh description of the reactor model is normally accomplished using from 150 to 250 radial intervals and 60 to 110 azimuthal intervals depending on the overall size of the reactor and on the

complexity required to model the core periphery, the in-vessel surveillance capsules, and the details of the reactor cavity. Mesh sizes are chosen to assure that proper convergence of the inner iterations is achieved on a pointwise basis. The pointwise inner iteration flux convergence criterion utilized in the r,θ calculations is set at a value of 0.001.

The mesh selection process results in a smaller spatial mesh in regions exhibiting steep gradients, in material zones of high cross-section (Σ_t), and at material interfaces. In the modeling of in vessel surveillance capsules, a minimum set of 3 radial by 3 azimuthal mesh are employed within the test specimen array to assure that sufficient information is produced for use in the assessment of fluence gradients within the materials test specimens, as well as in the determination of gradient corrections for neutron sensors. Additional radial and azimuthal mesh is employed to model the capsule structure surrounding the materials test specimen array. In modeling the stainless steel baffle region at the periphery of the core, a relatively fine spatial mesh is required to adequately describe this rectilinear component in r,θ geometry. In performing this x,y to r,θ transition, care is taken to preserve both the thickness and volume of the steel region in order to accurately address the shielding effectiveness of the component.

Although the example cited in this section is based on an octant symmetric model, the method is generally applicable even when such r,θ symmetry does not exist. The only change in the approach would be the use of a larger geometric model in the calculation.

As in the case of the r,θ model, the r,z model is also based on the use of nominal design dimensions and full power coolant densities. In this case, the homogenous core region is treated as an equivalent cylinder with a volume equal to that of the active core zone. The stainless steel former plates located between the core baffle and core barrel regions are also explicitly included in the model. The r,z geometric mesh description of the reactor model normally consists of from 130 to 230 radial intervals and from 90 to 150 axial intervals depending on the size of the reactor. Again, spatial mesh sizes are chosen to assure that proper convergence of the inner iterations was achieved on a pointwise basis. The pointwise inner iteration flux convergence criterion utilized in the r,z calculations is also set at a value of 0.001.

The one-dimensional radial model used in the synthesis procedure consists of the same radial spatial mesh array included in the r,z model. Thus, radial synthesis factors are easily determined on a mesh wise basis throughout the entire geometry.

2.3.2 Core Source

The spatial variation of the neutron source is generally obtained from a burnup weighted average of the respective power distributions from individual fuel cycles. These spatial distributions include pinwise gradients for all fuel assemblies located at the periphery of the core and typically include a uniform or flat distribution for fuel assemblies interior to the core. The spatial component of the neutron source is transposed from x,y to r,θ geometry by overlaying the mesh schematic to be used in the transport calculation on the pin by pin array and then computing the appropriate relative source applicable to each r,θ interval.

The x,y to r,θ transposition is accomplished by first defining a fine r,θ mesh working array. The Δr and $\Delta\theta$ of the fine mesh are usually chosen so that there is at least a 10x10 array of fine mesh over the area of

each fuel pin at the core periphery. The coordinates of the center of each fine mesh interval and its associated relative source strength are assigned to the fine mesh based on the pin that is coincident with the center of the fine mesh. In the limit as Δr and $\Delta\theta$ approach zero, this technique becomes an exact transformation.

Each space mesh in the r,θ transport geometry is checked to determine if it lies totally within the area of a particular fine r,θ working mesh. If it does, the relative source of that fine mesh is assigned to the transport space mesh. If, otherwise, the transport space mesh covers a part of one or more fine mesh, then the relative source assigned to the transport mesh is determined by an area weighting process as follows:

$$P_m = \frac{\sum_i A_i P_i}{\sum_i A_i}$$

where:

P_m = the relative source assigned to transport mesh m.

A_i = the area of fine working mesh i within transport mesh m.

P_i = the relative source within fine working mesh i.

The energy distribution of the source is determined by selecting a fuel burnup representative of conditions averaged over the irradiation period under consideration and an initial fuel assembly enrichment characteristic of the core designs used over the applicable period. From this average burnup, a fission split by isotope including ^{235}U, ^{238}U, ^{239}Pu, ^{240}Pu, ^{241}Pu, and ^{242}Pu is derived; and, from that fission split, composite values of energy release per fission, neutron yield per fission, and fission spectrum are determined. These composite values are then combined with the r,θ spatial distribution to produce the overall absolute neutron source for use in the transport calculations.

2.3.3 Validation of the Transport Calculations

The transport methodology described in Sections 2.3.1 and 2.3.2 of this report is identical to that described in the NRC approved version of WCAP-14040, Revision 4, Methodology Used to Develop Cold Overpressure Mitigation System Setpoints and RCS Heatup and Cooldown Limit Curves[26]. The validation of the transport methodology is based on the guidance provided in Regulatory Guide 1.190. In particular, the validation consists of the following stages:

1. Comparisons of calculations with benchmark measurements from the Pool Critical Assembly (PCA) simulator at the Oak Ridge National Laboratory (ORNL).

2. Comparisons of calculations with surveillance capsule and reactor cavity measurements from the H. B. Robinson power reactor benchmark experiment.

3. An analytical sensitivity study addressing the uncertainty components resulting from important input parameters applicable to the plant specific transport calculations used in the exposure assessments.

4. Comparisons of calculations with a measurement database obtained from a large number of surveillance capsules withdrawn from a variety of pressurized water reactors.

At each subsequent application of the methodology, comparisons are made with plant specific dosimetry results to demonstrate that the plant specific transport calculations are consistent with the uncertainties derived from the methods qualification.

The first stage of the methods validation addresses the adequacy of basic transport calculation and dosimetry evaluation techniques and associated cross-sections. This phase, however, does not test the accuracy of commercial core neutron source calculations nor does it address uncertainties in operational or geometric variables that affect power reactor calculations. The second stage of the validation addresses uncertainties that are primarily methods related and would tend to apply generically to all fast neutron exposure evaluations. The third stage of the validation identifies the potential uncertainties introduced into the overall evaluation due to calculational methods approximations as well as to a lack of knowledge relative to various plant specific parameters. The overall calculational uncertainty is established from the results of these three stages of the validation process.

The following summarizes the uncertainties determined from the results of the first three stages of the validation process:

PCA Benchmark Comparisons	3%
H. B. Robinson Benchmark Comparisons	3%
Analytical Sensitivity Studies	11%
Internals Dimensions	3%
Vessel Inner Radius	5%
Water Temperature	4%
Peripheral Assembly Source Strength	5%
Axial Power Distribution	5%
Peripheral Assembly Burnup	2%
Spatial Distribution of the Source	4%
Other Factors	5%

The category designated "Other Factors" is intended to attribute an additional uncertainty to other geometrical or operational variables that individually have an insignificant effect on the overall uncertainty, but collectively should be accounted for in the assessment.

The uncertainty components tabulated above represent percent uncertainty at the 1σ level. In the tabulation, the net uncertainty of 11% from the analytical sensitivity studies has been broken down into its individual components. When the four uncertainty values listed above (3%, 3%, 11%, and 5%) are combined in quadrature, the resultant overall 1σ calculational uncertainty is estimated to be 13%.

To date, the methodology described in Section 2.3 combined with the BUGLE-96 cross-section library has been used in the evaluation of dosimetry sets from 134 surveillance capsules, from 35 pressurized water reactors. These withdrawals consisted of 2 to 5 capsules from individual reactors. The comparisons of the plant specific calculations with the results of the capsule dosimetry are used to further validate the calculational methodology within the context of a 1σ calculational uncertainty of 13%.

2.3.4 Uncertainty Input to the Least Squares Adjustment

The neutron spectrum input to the least squares adjustment procedure is obtained directly from the results of plant-specific transport calculations for each sensor location. The spectrum at each location is input in an absolute sense (rather than as simply a relative spectral shape). Therefore, within the constraints of the assigned uncertainties, the calculated data are treated equally with the measurements. The input uncertainties associated with the calculated spectrum must be consistent with the benchmarking results discussed in Section 2.3.3.

The uncertainty matrix for the calculated spectrum is constructed from the following relationship:

$$M_{g'g} = R_n^2 + R_g * R_{g'} * P_{g'g}$$

where R_n specifies an overall fractional normalization uncertainty and the fractional uncertainties $R_{g'}$ and R_g specify additional random groupwise uncertainties that are correlated with a correlation matrix given by:

$$P_{g'g} = [1-\theta]\,\delta_{g'g} + \theta\, e^{-H}$$

where

$$H = \frac{(g-g')^2}{2\gamma^2}$$

The first term in the correlation matrix equation specifies purely random uncertainties, whereas the second term describes the short range correlations over a group range γ (θ specifies the strength of the latter term). The value of δ is 1.0 when g = g' and 0.0 otherwise.

The normalization uncertainty pertains primarily to the magnitude of the spectrum, whereas the groupwise uncertainties pertain to the shape of the spectrum relative to energy. A typical set of parameters defining the input uncertainties for the calculated spectrum is as follows:

Flux Normalization Uncertainty (R_n)	15%
Flux Group Uncertainties (R_g, $R_{g'}$)	
(E > 0.0055 MeV)	15%
(0.68 eV < E < 0.0055 MeV)	29%
(E < 0.68 eV)	52%
Short Range Correlation (θ)	
(E > 0.0055 MeV)	0.9
(0.68 eV < E < 0.0055 MeV)	0.5
(E < 0.68 eV)	0.5
Flux Group Correlation Range (γ)	
(E > 0.0055 MeV)	6
(0.68 eV < E < 0.0055 MeV)	3
(E < 0.68 eV)	2

These uncertainty assignments provide an input covariance matrix that is consistent with the calculational uncertainties defined through the benchmarking process.

2.4 REACTION RATE MEASUREMENT AND UNCERTAINTIES

Measurements at operating power reactors are generally accomplished with comprehensive multiple foil sensor sets including radiometric monitors (RM) and, in some instances for ex vessel monitoring, solid state track recorders (SSTR). In general, sensor sets employed in Westinghouse dosimetry programs include materials in which the following reactions can be measured:

In-Vessel		**Ex-Vessel**	
$^{63}Cu(n,\alpha)^{60}Co$		$^{63}Cu(n,\alpha)^{60}Co$	(Cd Covered)
$^{46}Ti(n,p)^{46}Sc$		$^{46}Ti(n,p)^{46}Sc$	(Cd Covered)
$^{54}Fe(n,p)^{54}Mn$		$^{54}Fe(n,p)^{54}Mn$	(Cd Covered)
$^{58}Ni(n,p)^{58}Co$		$^{58}Ni(n,p)^{58}Co$	(Cd Covered)
$^{238}U(n,f)FP$	(Cd Covered)	$^{238}U(n,f)FP$	(Cd Covered)
$^{237}Np(n,f)FP$	(Cd Covered)	$^{237}Np(n,f)FP$	(Cd Covered)
$^{59}Co(n,\gamma)^{60}Co$		$^{59}Co(n,\gamma)^{60}Co$	
$^{59}Co(n,\gamma)^{60}Co$	(Cd Covered)	$^{59}Co(n,\gamma)^{60}Co$	(Cd Covered)

These sensor sets provide adequate spectrum coverage in the fast neutron energy range greater than approximately 0.5 MeV and also include bare and cadmium covered cobalt sensors to provide an assessment of the thermal neutron flux at the measurement locations. These sensor sets are fully consistent with the guidance specified in Section 2.1.1 of Regulatory Guide 1.190. Similar sensor set designs are also utilized by other vendors of LWR dosimetry programs.

Following irradiation, the specific activity of each of the radiometric sensors is determined using the latest version of ASTM counting procedures for each reaction. In particular, the following standards are applicable to the radiometric sensors typically used in LWR programs:

E523 Standard Test Method for Measuring Fast Neutron Reaction Rates by Radioactivation of Copper.

E526 Standard Test Method for Measuring Fast Neutron Reaction Rates by Radioactivation of Titanium.

E263 Standard Test Method for Measuring Fast Neutron Reaction Rates by Radioactivation of Iron.

E264 Standard Test Method for Measuring Fast Neutron Reaction Rates by Radioactivation of Nickel.

E704 Standard Test Method for Measuring Fast Neutron Reaction Rates by Radioactivation of Uranium-238.

E705 Standard Test Method for Measuring Fast Neutron Reaction Rates by Radioactivation of Neptunium-237.

E481 Standard Test Method for Measuring Neutron Fluence Rate by Radioactivation of Cobalt and Silver.

E1005 Standard Method for Application and Analysis of Radiometric Monitors for Reactor Vessel Surveillance.

E481 Standard General Methods for Detector Calibration and Analysis of Radionuclides.

Following sample preparation and weighing, the specific activity of each sensor is determined using a germanium gamma spectrometer. In the case of multiple foil sensor sets, these analyses are usually completed by direct counting of each of the individual sensors, or, as is sometimes the case with ^{238}U and ^{237}Np fission monitors from in-vessel irradiations, by direct counting preceded by dissolution and chemical separation of cesium from the sensor.

For ex-vessel dosimetry irradiations, gradient chains or wires are often included with the multiple foil sensor sets. For these gradient measurements, individual sensors are obtained by cutting the chains into a series of segments to provide data at appropriate intervals over the extent of the beltline region of the pressure vessel. The determination of sensor specific activities in these segments then proceeds in the same fashion as for individual foils from the multiple foil sensor sets. In general, data from the following reactions are obtained from the gradient chain measurements:

$$^{54}Fe(n,p)^{54}Mn$$
$$^{58}Ni(n,p)^{58}Co$$
$$^{59}Co(n,\gamma)^{60}Co$$

These data can be used in conjunction with high purity foil measurements to provide mappings of the neutron environment external to the reactor pressure vessel.

Solid state track recorders (SSTR) have also been used for the measurement of fission reaction rates at ex-vessel dosimetry locations. The determination of reaction rates from these sensors is performed in accordance with the following ASTM standard:

E854 Standard test Method for Application and Analysis of Solid State Track Recorder (SSTR) Monitors for Reactor Surveillance.

In the SSTR analysis, the individual track recorders are optically scanned to determine the total number of fissions that occurred during the course of the irradiation. Because the scanning procedure results in an integral quantity representative of the entire irradiation, no radioactive decay corrections are required to determine the sensor reaction rates.

The individual radiometric and SSTR measurement data obtained from the counting laboratories, the physical characteristics of the sensors, and the operating history of the reactor are used to determine full power reaction rates characteristic of the irradiation period experienced by the foil sets. Generally, the reactor operating history data are obtained on a monthly basis for the sensor irradiation period. For the sensor sets used in both in-vessel and ex-vessel monitoring, the half lives of the product isotopes are long enough that a monthly histogram describing reactor operation has proven to be an adequate representation for use in radioactive decay corrections.

For the radiometric sensors used in LWR irradiations, reaction rates referenced to full power operation are determined from the following equation:

$$R = \frac{A}{N_o F Y \sum_{j=1}^{n} \frac{P_j}{P_{ref}} C_j (1 - e^{-\lambda t_j}) e^{\lambda t_d}}$$

where:

A	=	measured specific activity (dps/g)
R	=	sensor reaction rate averaged over the irradiation period and referenced to operation at a core power level of P_{ref} (rps/atom)
N_0	=	number of target element atoms per gram of sensor (atom/g)
F	=	weight fraction of the target isotope in the target material
Y	=	number of product atoms produced per reaction
P_j	=	average core power level during irradiation period j (MW)
P_{ref}	=	maximum or reference core power level of the reactor (MW)
C_j	=	calculated ratio of ϕ (E > 1.0 MeV) during irradiation period j to the time weighted average ϕ (E > 1.0 MeV) over the entire irradiation period
λ	=	decay constant of the product isotope (s^{-1})
t_j	=	length of irradiation period j (s)
t_d	=	decay time following irradiation period j (s)

and the summation is carried out over the total number of monthly intervals comprising the irradiation period.

In the above equation, the ratio P_j/P_{ref} accounts for month by month variation of power level within a given fuel cycle. The ratio C_j is calculated for each fuel cycle using the neutron transport methodology described in Section 2.3 of this report and accounts for the change in sensor reaction rates caused by variations in flux level due to changes in core power spatial distributions from fuel cycle to fuel cycle. For a single cycle irradiation, $C_j = 1.0$. However, for multiple fuel cycle irradiations, particularly those using low leakage fuel management, the additional C_j correction must be utilized. This additional correction can

be quite significant for sensor sets that have been irradiated for many fuel cycles in a reactor that has transitioned from non-low leakage to low leakage fuel management.

Because SSTR sensors are integrating devices not susceptible to radioactive decay of a product isotope, measurements of fissions per target atom, A, are converted directly to reaction rates using the following equation:

$$R = \frac{A}{\sum \frac{P_j * t_j}{P_{ref}}}$$

where the denominator in the above equation represents the total effective full power seconds (EFPS) of reactor operation during the irradiation period of the solid state track recorders.

Prior to using the measured reaction rates for direct comparison with the results of transport calculations or as input to the least squares adjustment procedure, additional corrections must be made to ^{238}U measurements to account for the presence of ^{235}U impurities in the sensors and for the build-in of plutonium isotopes over the course of the irradiation. These corrections are location and fluence dependent, are obtained from a combination of calculated data from the plant specific discrete ordinates analysis described in Section 2.3 of this report and, when available, measurements are made with ^{235}U foils or solid state track recorders.

In addition to the corrections for competing neutron induced reactions in the ^{238}U sensors, corrections must also be made to both the ^{238}U and ^{237}Np sensor reaction rates to account for gamma-ray induced fission reactions that occur during the irradiation. These photo-fission corrections are also location dependent and are obtained from the transport calculational methodology discussed in Section 2.3.

Typical corrections to the measured fission rates at in-vessel and ex-vessel sensor locations are summarized as follows:

	Typical Correction	
	In-Vessel	**Ex-Vessel**
^{235}U Impurities	8-12%	0-15%
Pu Build-In	7-20%	<1%
$^{238}U(\gamma,f)$	4-6%	3-5%
$^{237}Np(\gamma,f)$	1-2%	<1%

The corrections listed are typical values for a PWR plant with in-vessel capsules mounted on the outer radius of the thermal shield. These values cannot be used with a plant-specific sensor set. Rather, the appropriate corrections must be determined for each sensor set based on the actual plant specific geometry and irradiation history.

Along with the reaction rates, the uncertainty associated with each of these measurements is also an important input to the least squares adjustment procedure. The overall uncertainty in the measured reaction rates includes components due to the basic measurement process, the irradiation history corrections, and the corrections for competing reactions. A high level of accuracy in the reaction rate determinations is assured by using laboratory procedures that conform to the ASTM National Consensus Standards listed earlier in this section. In all cases, the latest available versions of the applicable standards are used in the dosimetry evaluations.

From these standards, the achievable uncertainties in the measured specific activities of each of the sensors comprising typical LWR multiple foil sensor sets are as follows:

Reaction	Precision	Bias
$^{63}Cu(n,\alpha)^{60}Co$	1%	3%
$^{46}Ti(n,p)^{46}Sc$	1%	3%
$^{54}Fe(n,p)^{54}Mn$	1%	3%
$^{58}Ni(n,p)^{58}Co$	1%	3%
$^{238}U(n,f)FP$	1%	5%
$^{237}Np(n,f)FP$	1%	5%
$^{59}Co(n,\gamma)^{60}Co$	1%	5%

These uncertainties included the effects of counting statistics, sample weighing, detector calibration, source/detector geometry corrections, and product nuclide branching ratios.

In determining reaction rates from the measured specific activities, the following additional uncertainties are incurred:

Reaction	Fission Yield	Product Half-Life	Competing Reactions
$^{63}Cu(n,\alpha)^{60}Co$		0.02%	
$^{46}Ti(n,p)^{46}Sc$		0.2%	
$^{54}Fe(n,p)^{54}Mn$		0.2%	
$^{58}Ni(n,p)^{58}Co$		0.2%	
$^{238}U(n,f)FP$	1%	0.1%	4%
$^{237}Np(n,f)FP$	2%	0.1%	1%
$^{59}Co(n,\gamma)^{60}Co$		0.02%	

After combing all of these uncertainty components, the sensor reaction rates derived from the counting and data evaluation procedures typically result in the following net uncertainties associated with the sensor reaction rates that are input to the least squares evaluation:

Reaction	Reaction Rate Uncertainty (1σ)
$^{63}Cu(n,\alpha)^{60}Co$	5%
$^{46}Ti(n,p)^{46}Sc$	5%
$^{54}Fe(n,p)^{54}Mn$	5%
$^{58}Ni(n,p)^{58}Co$	5%
$^{238}U(n,f)FP$	10%
$^{237}Np(n,f)FP$	10%
$^{59}Co(n,\gamma)^{60}Co$	5%

In addition to the adherence to ASTM National Consensus Standards in the evaluation of sensor reaction rates, the procedures used by Westinghouse have been periodically tested via round robin counting exercises included as part of the NRC sponsored Light Water Reactor Surveillance Dosimetry Improvement Program (LWR_SDIP) as well as by evaluation of fluence counting standards provided by the National Institute of Science and Technology (NIST). A summary of the results of these counting validations is as follows:

1980 Round robin counting of the foil sets irradiated at the Thermal Shield Back (TSB) and Pressure Vessel Face (PVF) positions of the PCA simulator.

1981 Round robin counting of additional foil sets included in the first metallurgical simulated surveillance capsule, also irradiated in the PCA benchmark mockup.

These two counting exercises involved direct comparisons with measurements obtained by the Hanford Engineering Development Laboratory (HEDL). At the time of these irradiations, HEDL was a prime contractor providing measurement services for the PCA benchmark and was cross calibrated with NIST and the MOL laboratory in Belgium.

1985 Counting and evaluation of $^{46}Ti(n,p)^{46}Sc$, $^{54}Fe(n,p)^{54}Mn$, and $^{58}Ni(n,p)^{58}Co$ certified fluence standards supplied by NIST.

Comparisons with fluence standards involve the determination not only of the reaction rate of each foil, but also of the spectrum averaged cross-section in the NIST ^{235}U irradiation facility. Thus, the comparisons with certified fluence standards test both the measurement process and the energy dependent reaction cross-sections used in the evaluation.

1992 Counting of NIST foils irradiated in an ex-vessel dosimetry experiment at the Trojan power reactor.

This exercise involved duplicate counting of a subset of irradiated foils by both Westinghouse and NIST to assure adequate cross-calibration of the laboratories so that data could be confidently mixed in the overall fluence evaluations performed by NIST and the Oak Ridge National Laboratory (ORNL).

1998 Round robin counting of ^{238}U and ^{237}Np certified fluence standards irradiated by NIST in the MDRF facility at the University of Michigan.

As in the case of the 1985 radiometric sensor evaluations, the fluence standard involved the determination of the reaction rate of each sensor, but also of the spectrum averaged cross-sections in the MDRF facility.

The results obtained from these counting comparisons are summarized as follows:

	[West]/[HEDL]		[West]/[NIST]			Average
	1980	1981	1985	1992	1995	
$^{63}Cu(n,\alpha)^{60}Co$	1.041	1.018		0.969		1.009
$^{46}Ti(n,p)^{46}Sc$	1.036		1.012	1.030		1.026
$^{54}Fe(n,p)^{54}Mn$	1.006	1.008	1.011	1.056		1.020
$^{58}Ni(n,p)^{58}Co$	1.006	0.990	1.028	1.029		1.013
$^{238}U(n,f)FP$	1.014	1.014			1.017	1.015
$^{237}Np(n,f)FP$	1.006	1.017			1.097	1.040
$^{59}Co(n,\gamma)^{60}Co$	1.017	1.017				1.017

These comparisons demonstrate that the procedures used by Westinghouse in the determination of sensor reaction rates have produced accurate and stable results over an extended period of time. The cross-comparisons with HEDL and NIST support the reaction rate uncertainties used by Westinghouse in performing LWR fluence evaluations.

In addition to these periodic comparisons, laboratory calibrations with NIST supplied sources are also carried out on a routine basis.

2.5 DOSIMETRY CROSS-SECTIONS AND UNCERTAINTIES

The third key set of input data for the least squares procedure includes the reaction cross-sections for each of the sensors included in the multiple foil dosimetry packages. The reaction rate cross-sections used by Westinghouse are taken from the SNLRML library[23]. This data library provides reaction cross-sections and associated uncertainties, including covariances, for 66 dosimetry sensors in common use. Both the cross-sections and the uncertainties are provided in a fine multi-group structure for use in least squares adjustment applications.

These cross-sections were compiled from the most recent cross-section evaluations including ENDF/B-VI and IRDF-90[24] and have been tested with respect to their accuracy and consistency for least squares analyses. Further, the library has been empirically tested for use in fission spectra determination as well as in the fluence and energy characterization of 14 MeV neutron sources. Detailed discussions of the contents of the SNLRML library along with the evaluation process for each of the sensors is provided in Reference 23.

For the sensors of interest to LWR dosimetry applications, the following uncertainties in the fission spectrum averaged cross-sections are provided in the SNLRML documentation package:

Reaction	Uncertainty (1σ)
$^{63}Cu(n,\alpha)^{60}Co$	4.08-4.16%
$^{46}Ti(n,p)^{46}Sc$	4.51-4.87%
$^{54}Fe(n,p)^{54}Mn$	3.05-3.11%
$^{58}Ni(n,p)^{58}Co$	4.49-4.56%
$^{238}U(n,f)FP$	0.54-0.64%
$^{237}Np(n,f)FP$	10.32-10.97%
$^{59}Co(n,\gamma)^{60}Co$	0.79-3.59%

These tabulated ranges provide an indication of the dosimetry cross-section uncertainties associated with typical sensor sets used in LWR irradiations.

3 TESTING OF THE FERRET PROCESSING PROCEDURES

As noted in Section 2 of this report, the FERRET least squares adjustment code is used by Westinghouse to combine the results of plant specific neutron transport calculations, dosimetry reaction cross-sections, and multiple foil reaction rate measurements to determine the best estimate values of damage exposure parameters (fluence [E > 1.0 MeV] and iron atom displacements [dpa]) along with their associated uncertainties at the measurement location.

As implemented in the FERRET analysis, the least squares evaluation of a given data set can be subdivided into the following two stages:

1. A pre-adjustment procedure performed by the SAND module that processes the calculated neutron spectrum and the SNLRML dosimetry cross-sections into the 53 energy group structure required by the FERRET module.

2. The subsequent application of the least squares algorithm in the FERRET module itself.

These two stages of the overall least squares adjustment procedure were individually tested by data comparisons in standard and benchmark fields as well as by analysis of a series of in-vessel and ex-vessel irradiations at operating power reactors.

In this section, results of least squares evaluations of dosimetry results from irradiations in the National Institute of Standards and Technology (NIST) Standard ^{235}U thermal fission field, the NIST Standard ^{252}Cf spontaneous fission field, the PCA simulator benchmark, and the H. B. Robinson power reactor benchmark are presented and discussed. In addition, results of the least squares evaluation of a database of in-vessel and ex-vessel power reactor measurements are described. These power reactor evaluations include data from a variety of different reactor designs and for several repeat measurement campaigns at individual reactors.

3.1 DATA COMPARISONS IN THE NIST ^{235}U FISSION FIELD

The sensor reaction cross-sections and associated uncertainties play a key role in the least squares evaluation of dosimetry data sets. Therefore, it is important to assess both the overall accuracy of these cross-sections and the impact on that accuracy of any data processing included in the evaluation procedure.

The least squares approach used by Westinghouse makes use of the SNLRML dosimetry cross-section library. This comprehensive library meets the requirements identified in ASTM E1018, "Standard Guide for Application of ASTM Evaluated Cross-Section Data File"[18] for use in LWR applications, and has been explicitly recommended in previous versions of the standard. The library is provided by the Radiation Safety Information Computational Center (RSICC) in a 640 neutron group format spanning an energy range from thermal to 20.0 MeV. Prior to use in the least squares adjustment, this fine group library is collapsed to a broad group structure consisting of 53 groups using the calculated neutron spectrum at the measurement location as a weighting function. The data comparisons from the standard field irradiations were used to determine the level of accuracy of the base cross-section library, as well as to demonstrate the adequacy of the collapsing procedure used to generate the 53 group library.

In ASTM E261, "Standard Practice for Determining Neutron Fluence, Fluence Rate, and Spectra by Radioactivation Techniques,"[19] fission spectrum averaged cross-sections applicable to the ^{235}U thermal fission field and the ^{252}Cf spontaneous fission field are provided for a variety of threshold activation detectors that are used in power and research reactor irradiations. In this data compilation, both calculated and measured spectrum averaged cross-sections are provided along with their evaluated uncertainties. The magnitude of errors in the processed dosimetry cross-section library can be judged by the observed disagreement between the calculated spectrum averaged cross-sections and the corresponding measured values for the standard ^{235}U and ^{252}Cf fields.

The data listed in Table 3-1 and Table 3-2 have been extracted from Table 3 of ASTM E261, and are representative of the foil sets used in power reactor irradiations and in the PCA benchmark irradiations. This subset of the ASTM E261 information includes the threshold reactions typically used in Light Water Reactor (LWR) surveillance capsule and ex-vessel dosimetry irradiations.

For the comparisons shown in Table 3-1 and Table 3-2, the authors of ASTM E261 based the calculated spectrum averaged reaction cross-sections on data from the recommended SNLRML library. Because the Westinghouse methodology and the evaluations provided in ASTM E261 are both based on the same dosimetry cross-section library, the calculated spectrum averaged cross-sections produced by the SAND/FERRET processing procedure should closely match the calculated values cited in the standard. Significant differences between the two sets of calculated spectrum averaged cross-sections would indicate errors in the processing procedure. Comparisons of the calculated spectrum averaged cross-sections from ASTM E261 with the corresponding cross-sections processed by Westinghouse are listed in Table 3-3.

The calculation to measurement comparisons given in Table 3-1 indicate that for the ^{235}U thermal fission field, the C/M ratios except $^{46}Ti(n,p)^{46}Sc$ fall within one standard deviation of the combined uncertainty in the calculation and measurement. For these reactions, the agreement between calculation and measurement is within 5%. In the case of the $^{46}Ti(n,p)^{46}Sc$ reaction, the C/M ratio falls within two standard deviations of the combined uncertainty with the calculation falling within 11% of the measured value.

For the ^{252}Cf spontaneous fission field, the comparisons provided in Table 3-2 show that, with the exception of the $^{238}U(n,f)FP$, $^{115}In(n,n')^{115m}$, and $^{46}Ti(n,p)^{46}Sc$ reactions, the C/M comparisons fall within one standard deviation of the combined uncertainty in the calculations and measurements. The C/M ratios for the $^{238}U(n,f)FP$, $^{115}In(n,n')^{115m}$ reactions fall within two standard deviations and the C/M ratio for the $^{46}Ti(n,p)^{46}Sc$ reaction falls within three standard deviations of the combined uncertainty. For reactions other than $^{46}Ti(n,p)^{46}Sc$, the agreement between calculation and measurement is within 6%. The calculated spectrum averaged cross-section for the $^{46}Ti(n,p)^{46}Sc$ reaction falls within 11% of the measured value.

The comparisons provided in Table 3-1 and Table 3-2 demonstrate that the SNLRML dosimetry cross-sections as processed by the authors of ASTM E261 produce accurate representations of the spectrum averaged cross-sections in the NIST standard fission fields. The Westinghouse least squares approach uses this same base dosimetry cross-section library, but a somewhat different processing procedure.

To compare the cross-section processing procedure used in the Westinghouse approach to expand the calculated input spectrum, spectrum weight the dosimetry cross-sections, and re-collapse the spectrum and dosimetry cross-sections to the FERRET 53 energy group structure, the ASTM E261 calculations for the ^{235}U thermal fission field were duplicated for the foil reactions contained in both the power reactor sensor set and PCA sensor set. In performing this calculation, the ENDF/B-VI ^{235}U fission spectrum supplied with the BUGLE-96 cross-section library was input to the SAND/FERRET procedure as the calculated spectrum. The dosimetry cross-sections for were taken directly from the SNLRML library.

Comparisons of the Westinghouse-processed spectrum averaged cross-sections with the calculated values from ASTM E261 are listed in Table 3-3 for both the power reactor and PCA sensor sets. An examination of the data given in Table 3-3 shows that the spectrum averaged cross-sections calculated by Westinghouse using the SAND pre-processing module are essentially identical to the calculated values given in ASTM E261, with the largest difference being at the 1% level.

The comparison results summarized in Table 3-3 combined with the C/M results listed in Table 3-1 and Table 3-2 demonstrate that using the SNLRML dosimetry cross-section library combined with the algorithms included in the SAND pre-processing module to produce a spectrum weighted broad group library, results in an appropriate cross-section representation for use in the FERRET least squares adjustment algorithm.

Table 3-1
^{235}U Fission Spectrum Averaged Cross-Sections from ASTM E261

Typical Power Reactor Sensor Sets			
Reaction	Spectrum Average Cross-Section (millibarns)		C/M
	Calculation	Measurement	
$^{63}Cu(n,\alpha)^{60}Co$	0.521 (2.85%, 6.05%)	0.50 (11.0%)	1.042 (12.87%)
$^{46}Ti(n,p)^{46}Sc$	10.43 (2.46%, 5.4%)	11.6 (3.45%)	0.899 (6.86%)
$^{54}Fe(n,p)^{54}Mn$	80.18 (2.17%, 4.69%)	80.5 (2.86%)	0.996 (5.91%)
$^{58}Ni(n,p)^{58}Co$	105.69 (2.43%, 4.52%)	108.5 (5.0%)	0.974 (7.16%)
$^{238}U(n,f)FP$	306.23 (0.53%, 4.21%)	309.0 (2.6%)	0.991 (4.98%)
$^{237}Np(n,f)FP$	1330.1 (9.33%, 4.31%)	1344.0 (4.0%)	0.990 (11.0%)

PCA Sensor Sets			
Reaction	Spectrum Average Cross-Section (millibarns)		C/M
	Calculation	Measurement	
$^{27}Al(n,\alpha)^{24}Na$	0.727 (1.40%, 6.95%)	0.706 (3.97%)	1.030 (8.13%)
$^{58}Ni(n,p)^{58}Co$	105.69 (2.43%, 4.52%)	108.5 (5.0%)	0.974 (7.16%)
$^{115}In(n,n')^{115m}In$	186.35 (2.17%, 4.17%)	190.3 (3.84%)	0.979 (6.07%)
$^{103}Rh(n,n')^{103m}Rh$	706.02 (3.1%, 4.14%)	733.0 (5.2%)	0.963 (7.33%)
$^{238}U(n,f)FP$	306.23 (0.53%, 4.21%)	309.0 (2.6%)	0.991 (4.98%)
$^{237}Np(n,f)FP$	1330.1 (9.33%, 4.31%)	1344.0 (4.0%)	0.990 (11.0%)

Notes:

1. The tabulated data were taken from Table 3 of ASTM E261.

2. For the calculated values, the cross-section and spectrum components of the uncertainty, respectively, are shown in parentheses.

3. The measurement uncertainty is also shown in parentheses.

4. The uncertainty in the C/M ratio represents a sum in quadrature of the measurement and calculational uncertainty.

Table 3-2
^{252}Cf Fission Spectrum Averaged Cross-Sections from ASTM E261

Typical Power Reactor Sensor Sets			
Reaction	Spectrum Average Cross-Section (millibarns)		C/M
	Calculation	Measurement	
$^{63}Cu(n,\alpha)^{60}Co$	0.678 (2.83%, 1.38%)	0.689 (1.98%)	0.984 (3.72%)
$^{46}Ti(n,p)^{46}Sc$	12.56 (2.45%, 1.18%)	14.09 (1.76%)	0.891 (3.24%)
$^{54}Fe(n,p)^{54}Mn$	88.12 (2.14%, 0.79%)	86.92 (1.34%)	1.014 (2.65%)
$^{58}Ni(n,p)^{58}Co$	115.31 (2.40%, 0.73%)	117.6 (1.3%)	0.981 (2.83%)
$^{238}U(n,f)FP$	315.39 (0.53%, 0.4%)	325.0 (1.63%)	0.970 (1.76%)
$^{237}Np(n,f)FP$	1335.0 (9.2%, 0.23%)	1361.0 (1.58%)	0.981 (9.43%)

PCA Sensor Sets			
Reaction	Spectrum Average Cross-Section (millibarns)		C/M
	Calculation	Measurement	
$^{27}Al(n,\alpha)^{24}Na$	1.04 (1.36%, 1.61%)	1.017 (1.47%)	1.019 (2.57%)
$^{58}Ni(n,p)^{58}Co$	115.31 (2.40%, 0.73%)	117.6 (1.3%)	0.981 (2.83%)
$^{115}In(n,n')^{115m}In$	189.8 (2.16%, 0.38%)	197.6 (1.3%)	0.961 (2.55%)
$^{103}Rh(n,n')^{103m}Rh$	714.45 (3.08%, 0.27%)	757.0 (4.0%)	0.944 (5.06%)
$^{238}U(n,f)FP$	315.39 (0.53%, 0.4%)	325.0 (1.63%)	0.970 (1.76%)
$^{237}Np(n,f)FP$	1335.0 (9.2%, 0.23%)	1361.0 (1.58%)	0.981 (9.43%)

Notes:

1. The tabulated data were taken from Table 3 of ASTM E261.

2. For the calculated values, the cross-section and spectrum components of the uncertainty, respectively, are shown in parentheses.

3. The measurement uncertainty is also shown in parentheses.

4. The uncertainty in the C/M ratio represents a sum in quadrature of the measurement and calculational uncertainty.

Table 3-3
Comparison of Calculated ^{235}U Fission Spectrum Averaged Cross-Sections

Typical Power Reactor Sensor Sets			
Reaction	Spectrum Average Cross-Section (millibarns)		Ratio
	ASTM E261	SAND/FERRET	FERRET/E261
$^{63}Cu(n,\alpha)^{60}Co$	0.521	0.523	1.004
$^{46}Ti(n,p)^{46}Sc$	10.4	10.3	0.990
$^{54}Fe(n,p)^{54}Mn$	80.2	80.3	1.001
$^{58}Ni(n,p)^{58}Co$	106	106	1.000
$^{238}U(n,f)FP$	306	306	1.000
$^{237}Np(n,f)FP$	1330	1330	1.000

PCA Sensor Sets			
Reaction	Spectrum Average Cross-Section (millibarns)		Ratio
	ASTM E261	SAND/FERRET	FERRET/E261
$^{27}Al(n,\alpha)^{24}Na$	0.727	0.729	1.003
$^{58}Ni(n,p)^{58}Co$	106	106	1.000
$^{115}In(n,n')^{115m}In$	186	186	1.000
$^{103}Rh(n,n')^{103m}Rh$	706	706	1.000
$^{238}U(n,f)FP$	306	306	1.000
$^{237}Np(n,f)FP$	1330	1330	1.000

3.2 EVALUATION OF THE PCA SIMULATOR BENCHMARK

The guidance provided in Regulatory Guide 1.190[3] recommends using measured data from the Pool Critical Assembly (PCA) pressure vessel simulator[13, 20, 21] to benchmark neutron transport calculational methods for application to LWR pressure vessel fluence determination. The documentation describing the PCA experimental program and the subsequent evaluation of the dosimetry data obtained from the simulator irradiations also allows a comparison of results from the Westinghouse least squares methodology using the FERRET code with similar analyses completed by other laboratories. These comparisons are valuable because they show any differences that may occur due to using different input or different least squares adjustment codes.

In Reference 20, several least squares evaluations of dosimetry data from the PCA 12/13 configuration were documented. These evaluations were completed by Rolls Royce and Associates (RR&A), Hanford Engineering Development Laboratory (HEDL), and Oak Ridge National Laboratory (ORNL), each using a different least squares adjustment code. The results of these least squares analyses were used to establish recommended values of key neutron exposure parameters (ϕ (E > 1.0 MeV) and dpa) for this blind test configuration.

A plan view of the PCA reactor and pressure vessel simulator showing materials characteristic of the core axial midplane is shown in Figure 3-1. The configuration shown in Figure 3-1 was developed from dimensional information provided in Reference 13, and uses the latest available geometric data for the simulator. During the PCA experiments, measurements were taken at several locations within the mockup to provide traverse data extending from the reactor core outward through the pressure vessel simulator and into the void box. The specific measurement locations are illustrated on Figure 3-1 and listed in Table 3-4. The measurements of interest were obtained on the lateral centerline of the mockup at an elevation opposite the axial midplane of the simulator.

The measurement locations specified in Table 3-4 provide data sufficient to generate calculation/measurement comparisons throughout the entire 12/13 configuration. The data afford the opportunity for comparisons over a wide attenuation range with a changing neutron energy spectrum within the carbon steel simulator wall. Thus, this simulator benchmark experiment provides an excellent test for the evaluation of transport calculation and dosimetry evaluation methodologies for both in-vessel and ex-vessel irradiations.

The least squares evaluations documented in Reference 20 included data from a subset of the measurement points listed in Table 3-4. In particular, least squares comparisons were provided at locations A2, A4, A5, A6, and A7. These data locations were intended to simulate an in-vessel surveillance capsule mounted on the outer diameter of the thermal shield, the 1/4T, 1/2T, and 3/4T locations interior to the pressure vessel wall, and an ex-vessel dosimetry location in the reactor cavity external to the pressure vessel wall.

The Reference 20 analyses were completed using three different least squares adjustment codes (SENSAK[22], FERRET[5], and LSL-M2[9]). The calculated input spectra for the SENSAK analysis were based on discrete ordinates calculations using the EUROLIB-4 cross-section library. The FERRET and LSL-M2 analyses likewise used calculated spectra from discrete ordinates calculations, but based on the use of the ENDF/B-IV SAILOR cross-section library. All of these least squares evaluations used the

recommended measurement data from the PCA irradiations and dosimetry reaction cross-sections from the ENDF/B-V data files.

The least squares results provided in Section 7.1 of Reference 20 are reproduced in Table 3-5. The data included in Table 3-5 show that, in terms of adjusted neutron flux (E > 1.0 MeV), the RR&A and HEDL analyses produce essentially identical results, whereas the ORNL evaluation yields adjusted results that are lower by 4.0% to 8.5%. However, the reported results are consistent within the combined uncertainties quoted for the adjusted results. Thus, these prior least squares evaluations of the PCA benchmark data did not indicate any significant differences in the adjustments produced by these three codes.

As a test of the current Westinghouse least squares methodology using the FERRET code, these PCA evaluations were repeated using updated input based on the now available ENDF/B-VI neutron transport and dosimetry reaction cross-section libraries. This updated evaluation tested the capabilities of the FERRET code as applied by Westinghouse using current methodology and data libraries.

Due to the relative small size of the PCA configuration, calculations using the typical 3D synthesis approach tend to break down at locations toward the back side of the simulator (A6, A7). Therefore, the spectrum input to the least squares analysis was taken from a fully three-dimensional calculation using the TORT code[10] run in X,Y,Z geometry. The TORT calculations were run using the BUGLE-96 cross-section library[11] with a P_3 scattering cross-section expansion and an S_8 angular quadrature. The uncertainty associated with the calculated spectrum was based on the formulation described in Section 2.3 of this report. The measured reaction rates used in the least squares evaluation of dosimetry sets from locations A1 through A7 within the PCA 12/13 configuration were the recommended values from Reference 20. The reaction rate uncertainties used in the analysis were 5% and 10% for the non fission and fission sensors, respectively. The dosimetry reaction cross-sections and cross-section uncertainty data were obtained from the SNLRML library[23].

Results of the FERRET least squares evaluations of the PCA dosimetry from locations A1 through A7 are shown in Table 3-6 through Table 3-9. In Table 3-6, comparisons of the measurement to calculation ratios for each sensor are listed before and after application of the least squares procedure. The comparisons before adjustment (M/C) show that the baseline calculation and the reaction rate measurements are in good agreement for all reactions at all measurement locations with the M/C values falling in a range of 0.91 to 1.05. The linear average of the M/C data at each measurement location ranges from 0.97 to 1.02, with the standard deviations in these averages varying from 2.0% to 4.8%. These M/C comparisons fall within the 15% standard deviation pertaining to the unadjusted calculation. In total, these comparisons indicate reasonable consistency between the calculated and measured reaction rates and imply that any adjustments to the calculated spectra should be relatively small.

The comparisons after adjustment (M/A) show that the adjustments are indeed small, but result in improved agreement between the calculated and measured data. After adjustment, the M/A data for the individual sensors fall in the range of 0.94 to 1.06, and the linear average of the M/A ratios at each measurement location ranges from 0.99 to 1.01. The standard deviations in these linear averages have been reduced, ranging from 1.05 to 3.6%.

In Table 3-7, the neutron flux (E > 1.0 MeV) at each measurement location is provided before and after adjustment. The data in Table 3-7 show that the net adjustment in the fast neutron flux was 3% or less,

depending on location and that the inclusion of the measurement information has reduced the uncertainty in the magnitude of the fast flux from 15% to 4%. This improved uncertainty in the fast neutron flux is consistent with the corresponding improvement in the calculated sensor reaction rates.

Detailed comparisons of the data adjustments for each measurement location are given in Table 3-8. These comparisons show that in all cases, the adjustments performed by the FERRET analysis are small and consistent with the input uncertainty bounds for the reaction rates and calculated neutron flux. The χ^2 per degree of freedom associated with each of the analyses indicate good data consistency for all cases.

Finally, in Table 3-9, the results of the current FERRET evaluation of the PCA data are compared with the prior analysis listed in Table 3-5. The newer FERRET results are essentially identical to the previous results reported by RR&A and HEDL, but with an improved uncertainty. The improvement in the uncertainty is attributable to greater accuracy in the input calculated spectra, which were based on ENDF/B-VI transport cross-sections rather than on the ENDF/B-IV data libraries that were available at the time of the initial evaluations.

The analyses summarized in Table 3-6 through Table 3-9 demonstrate that the FERRET code as applied by Westinghouse yields results consistent with those produced by other least squares adjustment codes for the PCA benchmark analyses. Further, the PCA evaluations show that the FERRET least squares analyses produced consistent results with no anomalous behavior for a wide range of neutron spectra characteristic of in-vessel and ex-vessel dosimetry locations as well as for locations interior to the carbon steel pressure vessel wall.

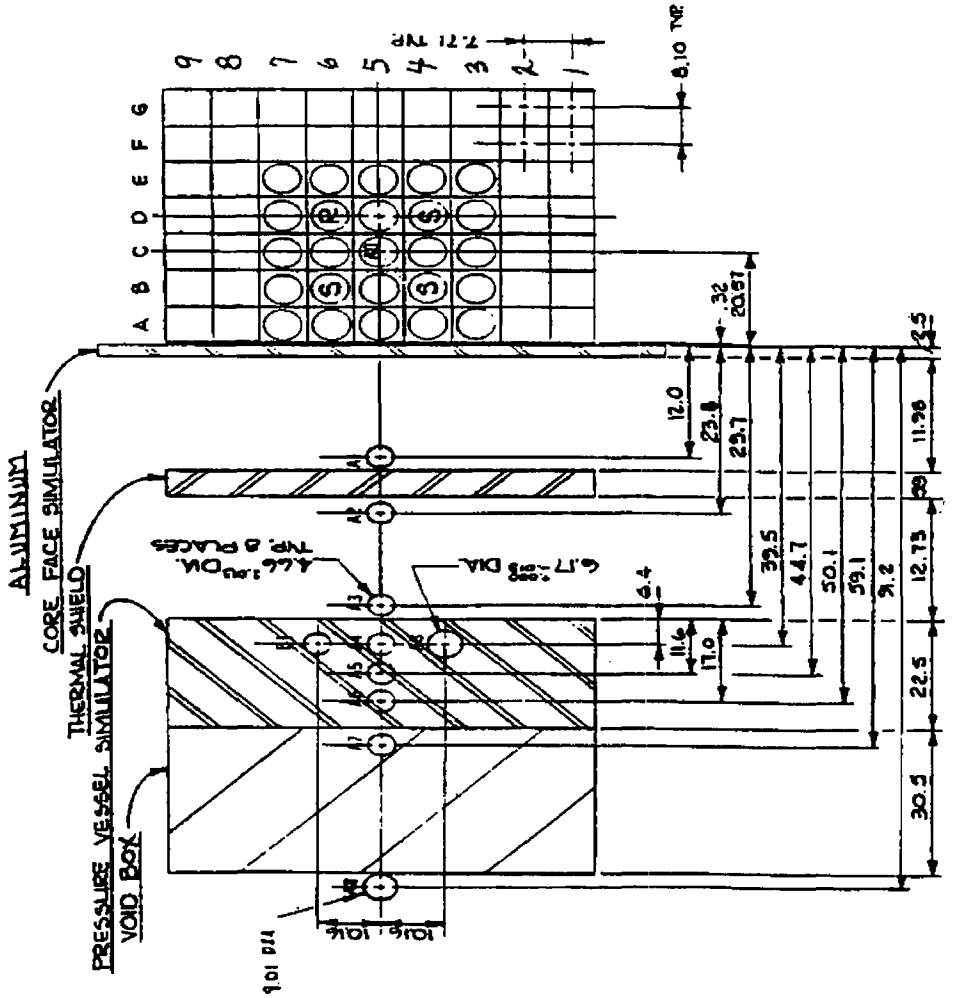

Figure 3-1 PCA 12/13 Configuration - X,Y Geometry
(Dimensions in centimeters)

Table 3-4
Summary of Measurement Locations Within the PCA 12/13 Configuration

Measurement Location	ID	Y(cm)
Core Center	A0	-20.57
Thermal Shield Front	A1	12.0
Thermal Shield Back	A2	23.8
Pressure Vessel Front	A3	29.7
Pressure Vessel 1/4T	A4	39.5
Pressure Vessel 1/2T	A5	44.7
Pressure Vessel 3/4T	A6	50.1
Void Box	A7	59.1

Table 3-5
Least Squares Adjusted Results for the PCA 12/13 Configuration
Participating Laboratory Data from NUREG/CR-3318

Location	RR&A		HEDL		ORNL	
	$\phi(E > 1.0)$	% std.	$\phi(E > 1.0)$	% std.	$\phi(E > 1.0)$	% std.
A2	4.01e-07	9			3.85e-07	8
A4	4.50e-07	7	4.58e-08	7	4.22e-08	4
A5	2.21e-07	7	2.21e-08	7	2.03e-08	4
A6	9.73e-09	8	9.82e-09	7	8.91e-09	4
A7	2.88e-09	43				

Table 3-6
M/C Comparisons for the PCA 12/13 Blind Test Experiment

Comparisons Before Adjustment

	M/C Ratio						
	A1	**A2**	**A3**	**A4**	**A5**	**A6**	**A7**
$^{27}Al(n,\alpha)^{24}Na$ (Cd)	1.00	1.00	0.95	0.96	0.97	0.98	
$^{58}Ni(n,p)^{58}Co$ (Cd)	1.04	1.02	0.99	1.00	1.01	0.96	
$^{115}In(n,n')^{115m}In$ (Cd)	1.04	1.02	0.96	0.96	0.99	0.99	1.04
$^{103}Rh(n,n')^{103m}Rh$ (Cd)	1.01	0.97	0.97	0.96	1.02	1.05	1.05
$^{238}U(n,f)FP$ (Cd)			0.91	1.00	1.02	1.05	1.04
$^{237}Np(n,f)FP$ (Cd)			1.05	0.99	0.98	1.01	0.96
Average	1.02	1.00	0.97	0.98	1.00	1.01	1.02
% Standard Deviation	2.0	2.4	4.8	2.1	2.1	3.7	4.1

Comparisons After Adjustment

	M/A Ratio						
	A1	**A2**	**A3**	**A4**	**A5**	**A6**	**A7**
$^{27}Al(n,\alpha)^{24}Na$ (Cd)	0.99	1.01	1.01	1.01	1.01	1.00	
$^{58}Ni(n,p)^{58}Co$ (Cd)	0.99	0.99	0.98	0.98	0.99	1.02	
$^{115}In(n,n')^{115m}In$ (Cd)	0.99	0.99	1.01	1.02	1.01	1.01	1.00
$^{103}Rh(n,n')^{103m}Rh$ (Cd)	1.01	1.02	1.00	1.01	0.99	0.99	0.99
$^{238}U(n,f)FP$ (Cd)			1.06	0.98	0.98	0.94	1.00
$^{237}Np(n,f)FP$ (Cd)			0.95	1.02	1.02	1.00	1.04
Average	0.99	1.00	1.00	1.00	1.00	0.99	1.01
% Standard Deviation	1.0	1.6	3.6	1.7	1.5	2.7	2.2

Table 3-7
Summary of Least Squares Adjustment Results for the PCA 12/13 Blind Test Experiment

Location	ϕ(E > 1.0 MeV) [n/cm^2-s]		A/C
	Calculated	Adjusted	
A1	3.77e-06 (15%)	3.88e-06 (4%)	1.03
A2	4.26e-07 (15%)	4.26e-07 (4%)	1.00
A3	1.42e-07 (15%)	1.38e-07 (4%)	0.97
A4	4.73e-08 (15%)	4.62e-08 (4%)	0.98
A5	2.24e-08 (15%)	2.25e-08 (4%)	1.00
A6	9.87e-09 (15%)	9.88e-09 (4%)	1.00
A7	2.72e-09 (15%)	2.81e-09 (4%)	1.03

Note: Numbers in parentheses represent one standard deviation.

Table 3-8
FERRET Results for the PCA 12/13 Blind Test Experiment

Location A1 (χ^2/Degree of Freedom = 0.03)

Reaction	Reaction Rate [rps/atom]			Adjustment % of Calc.
	Measured	Calculated	Adjusted	
$^{27}Al(n,\alpha)^{24}Na$ (Cd Cov)	5.48e-33	5.49e-33	5.53e-33	0.7
$^{58}Ni(n,p)^{58}Co$ (Cd Cov.)	6.31e-31	6.07e-31	6.23e-31	2.6
$^{115}In(n,n')^{115m}In$ (Cd Cov.)	1.05e-30	1.01e-30	1.04e-30	3.0
$^{103}Rh(n,n')^{103m}Rh$ (Cd Cov.)	4.06e-30	4.00e-30	4.10e-30	2.5
$^{238}U(n,f)FP$ (Cd Cov.)				
$^{237}Np(n,f)FP$ (Cd Cov.)				
ϕ(E >1.0 MeV) [n/cm^2-s]		3.77e-06	3.88e-06	2.9

Location A2 (χ^2/Degree of Freedom = 0.08)

Reaction	Reaction Rate [rps/atom]			Adjustment % of Calc.
	Measured	Calculated	Adjusted	
$^{27}Al(n,\alpha)^{24}Na$ (Cd Cov)	7.16e-34	7.14e-34	7.20e-34	0.8
$^{58}Ni(n,p)^{58}Co$ (Cd Cov.)	6.72e-32	6.57e-32	6.64e-32	1.1
$^{115}In(n,n')^{115m}In$ (Cd Cov.)	1.14e-31	1.12e-31	1.13e-31	0.9
$^{103}Rh(n,n')^{103m}Rh$ (Cd Cov.)	4.50e-31	4.64e-31	4.60e-31	-0.9
$^{238}U(n,f)FP$ (Cd Cov.)				
$^{237}Np(n,f)FP$ (Cd Cov.)				
ϕ(E >1.0 MeV) [n/cm^2-s]		4.26e-07	4.26e-07	0.2

Table 3-8 (Continued)
FERRET Results for the PCA 12/13 Blind Test Experiment

Location A3 (χ^2/Degree of Freedom = 0.13)

Reaction	Reaction Rate [rps/atom]			Adjustment % of Calc.
	Measured	Calculated	Adjusted	
$^{27}Al(n,\alpha)^{24}Na$ (Cd Cov)	3.13e-34	3.28e-34	3.15e-34	-4.0
$^{58}Ni(n,p)^{58}Co$ (Cd Cov.)	2.50e-32	2.53e-32	2.45e-32	-3.2
$^{115}In(n,n')^{115m}In$ (Cd Cov.)	3.68e-32	3.84e-32	3.72e-32	-3.1
$^{103}Rh(n,n')^{103m}Rh$ (Cd Cov.)	1.47e-31	1.52e-31	1.47e-31	-3.3
$^{238}U(n,f)FP$ (Cd Cov.)	5.91e-12	6.47e-32	6.27e-32	-3.1
$^{237}Np(n,f)FP$ (Cd Cov.)	3.05e-31	2.90e-31	2.91e-31	0.3
ϕ(E >1.0 MeV) [n/cm^2-s]		1.42e-07	1.38e-07	-2.9

Location A4 (χ^2/Degree of Freedom = 0.06)

Reaction	Reaction Rate [rps/atom]			Adjustment % of Calc.
	Measured	Calculated	Adjusted	
$^{27}Al(n,\alpha)^{24}Na$ (Cd Cov)	7.15e-35	7.46e-35	7.23e-35	-3.1
$^{58}Ni(n,p)^{58}Co$ (Cd Cov.)	5.69e-33	5.70e-33	5.58e-33	-2.1
$^{115}In(n,n')^{115m}In$ (Cd Cov.)	1.11e-32	1.15e-32	1.13e-32	-1.7
$^{103}Rh(n,n')^{103m}Rh$ (Cd Cov.)	5.67e-32	5.89e-32	5.70e-32	-3.2
$^{238}U(n,f)FP$ (Cd Cov.)	1.79e-32	1.79e-32	1.75e-32	-2.2
$^{237}Np(n,f)FP$ (Cd Cov.)	1.20e-31	1.21e-32	1.19e-32	-1.7
ϕ(E >1.0 MeV) [n/cm^2-s]		4.73e-08	4.62e-08	-2.4

Table 3-8 (Continued)
FERRET Results for the PCA 12/13 Blind Test Experiment

Location A5 (χ^2/Degree of Freedom = 0.04)

Reaction	Reaction Rate [rps/atom]			Adjustment % of Calc.
	Measured	Calculated	Adjusted	
$^{27}Al(n,\alpha)^{24}Na$ (Cd Cov)	2.92e-35	3.01e-35	2.94e-35	-2.3
$^{58}Ni(n,p)^{58}Co$ (Cd Cov.)	2.25e-33	2.24e-33	2.23e-33	-0.4
$^{115}In(n,n')^{115m}In$ (Cd Cov.)	5.20e-33	5.27e-33	5.27e-33	0.0
$^{103}Rh(n,n')^{103m}Rh$ (Cd Cov.)	3.24e-32	3.17e-32	3.22e-32	1.6
$^{238}U(n,f)FP$ (Cd Cov.)	7.88e-33	7.70e-33	7.70e-33	0.0
$^{237}Np(n,f)FP$ (Cd Cov.)	6.56e-32	6.71e-32	6.66e-32	-0.7
ϕ(E >1.0 MeV) [n/cm^2-s]		2.24e-08	2.25e-08	0.2

Location A6 (χ^2/Degree of Freedom = 0.04)

Reaction	Reaction Rate [rps/atom]			Adjustment % of Calc.
	Measured	Calculated	Adjusted	
$^{27}Al(n,\alpha)^{24}Na$ (Cd Cov)	1.12e-35	1.15e-35	1.12e-35	-2.6
$^{58}Ni(n,p)^{58}Co$ (Cd Cov.)	7.99e-34	8.29e-34	8.14e-34	-1.8
$^{115}In(n,n')^{115m}In$ (Cd Cov.)	2.23e-33	2.26e-33	2.25e-33	-0.4
$^{103}Rh(n,n')^{103m}Rh$ (Cd Cov.)	1.67e-32	1.60e-32	1.66e-32	3.7
$^{238}U(n,f)FP$ (Cd Cov.)	3.26e-33	3.09e-33	3.07e-33	-0.6
$^{237}Np(n,f)FP$ (Cd Cov.)	3.46e-32	3.43e-32	3.47e-32	1.2
ϕ(E >1.0 MeV) [n/cm^2-s]		9.87e-09	9.88e-09	0.1

Table 3-8 (Continued)
FERRET Results for the PCA 12/13 Blind Test Experiment

Location A7 (χ^2/Degree of Freedom = 0.04)

Reaction	Reaction Rate [rps/atom]			Adjustment % of Calc.
	Measured	Calculated	Adjusted	
$^{27}Al(n,\alpha)^{24}Na$ (Cd Cov)				
$^{58}Ni(n,p)^{58}Co$ (Cd Cov.)				
$^{115}In(n,n')^{115m}In$ (Cd Cov.)	6.43e-34	6.20e-34	6.40e-34	3.2
$^{103}Rh(n,n')^{103m}Rh$ (Cd Cov.)	4.83e-33	4.60e-33	4.80e-33	4.3
$^{238}U(n,f)FP$ (Cd Cov.)	8.65e-34	8.33e-34	8.61e-34	3.4
$^{237}Np(n,f)FP$ (Cd Cov.)	9.60e-33	9.97e-33	9.98e-33	0.1
ϕ(E >1.0 MeV) [n/cm^2-s]		2.72e-09	2.81e-09	3.2

Table 3-9
Comparison of Current FERRET Least Squares Results with Prior Analyses
PCA 12/13 Configuration

	FERRET		RR&A		HEDL		ORNL	
	ϕ(E>1.0)	% std.	ϕ(E>1.0)	% std.	ϕ(E>1.0)	% std.	ϕ(E>1.0)	% std.
A1	3.88e-06	4						
A2	4.26e-07	4	4.01e-07	9			3.85e-07	8
A3	1.38e-07	4						
A4	4.62e-08	4	4.50e-07	7	4.58e-08	7	4.22e-08	4
A5	2.25e-08	4	2.21e-07	7	2.21e-08	7	2.03e-08	4
A6	9.88e-09	4	9.73e-09	8	9.82e-09	7	8.91e-09	4
A7	2.81e-09	4	2.88e-09	43				

3.3 EVALUATION OF THE H. B. ROBINSON BENCHMARK

In performing the benchmarking of the neutron transport methodology described in Section 2.3 of this report, comparisons of calculations using ENDF/B-VI cross-sections with measured reaction rates from both in-vessel and ex-vessel dosimetry sets irradiated in the H. B. Robinson Cycle 9 benchmark experiment were used. This direct comparison of the calculated reaction rates with measurements showed excellent agreement. As a further demonstration of the application of the least squares procedure using the FERRET code, an evaluation of the in-vessel and ex-vessel data from the H. B. Robinson benchmark was also completed.

The neutron transport calculations input to the least squares analysis were completed using the standard synthesis approach described in Section 2.3 of this report. The calculations were run using the BUGLE-96 cross-section library[11] with a P_3 scattering cross-section expansion and an S_8 angular quadrature. The uncertainty associated with the calculated spectrum was likewise based on the formulation described in Section 2.3 of this report. The measured reaction rates used in the least squares evaluation of the dosimetry were the recommended values from Reference 25. The reaction rate uncertainties used in the analysis were 5% and 10% for the non fission and fission sensors, respectively. The dosimetry reaction cross-sections and cross-section uncertainty data were obtained from the SNLRML library[23].

Results of the least squares evaluation of the H. B. Robinson in-vessel and ex-vessel sensor sets are provided in Table 3-10 through Table 3-12. Detailed comparisons of the data adjustments for each measurement location are given in Table 3-10. These comparisons show that in both cases, the adjustments performed by the FERRET analysis are small and consistent with the input uncertainty bounds for the reaction rates and calculated neutron flux. The χ^2 per degree of freedom associated with each of the analyses indicate good data consistency for all cases.

In Table 3-11, the neutron flux (E > 1.0 MeV) at each measurement location is provided before and after adjustment. The data in Table 3-11 show that the net adjustment in the fast neutron flux was 1% for the in-vessel dosimetry and 2% for the ex-vessel data set. Further, the inclusion of the measurement information has reduced the uncertainty in the magnitude of the fast flux from 15% to 5% and 7% at the in-vessel and ex-vessel locations, respectively. This improved uncertainty in the fast neutron flux is consistent with the corresponding improvement in the calculated sensor reaction rates and with the FERRET analysis performed for the PCA data sets.

In Table 3-12, comparisons of the measurement to calculation ratios for each sensor are listed before and after application of the least squares procedure. The comparisons before adjustment (M/C) show that the baseline calculation and the reaction rate measurements are in good agreement for all reactions at all measurement locations with the M/C values falling in a range of 0.95 to 1.11. The linear average of the M/C data at both measurement locations is 1.03, with the standard deviations in these averages being 4.4% and 5.2% for the in-vessel and ex-vessel data, respectively. All of these M/C comparisons fall within the 15% standard deviation ascribed to the unadjusted calculation. In aggregate, these comparisons indicate reasonable consistency between the calculated and measured reaction rates and imply that any adjustments to the calculated spectra should be relatively small.

The comparisons after adjustment (M/A) show that the adjustments are indeed small, but do result in improved agreement between the calculated and measured data. After adjustment, the M/A data for the

individual sensors is improved and falls in the range of 0.96 to 1.09 and the linear average of the M/A ratios at both measurement location is 1.01. The standard deviations in these linear averages have been reduced, ranging from 3.6% at the in-vessel location to 5.0% in the reactor cavity.

The comparisons summarized in Table 3-10 through Table 3-12 support the analyses previously presented for the PCA benchmark experiment and further demonstrate the applicability of the FERRET code and the least squares procedure used by Westinghouse for analysis of LWR dosimetry data.

Table 3-10
FERRET Results for the H. B. Robinson Benchmark Experiment

In-Vessel (χ^2/Degree of Freedom = 0.23)

Reaction	Reaction Rate [rps/atom]			Adjustment % of Calc.
	Measured	Calculated	Adjusted	
$^{63}Cu(n,\alpha)^{60}Co$	3.98e-17	3.85e-17	3.97e-17	3.1
$^{46}Ti(n,p)^{46}Sc$	6.49e-16	6.07e-16	6.30e-16	3.8
$^{54}Fe(n,p)^{54}Mn$	3.83e-15	3.79e-15	3.84e-15	1.3
$^{58}Ni(n,p)^{58}Co$	4.88e-15	5.13e-15	5.10e-15	-0.6
$^{238}U(n,p)FP$	1.80e-14	1.68e-14	1.69e-14	0.6
$^{237}Np(n,p)FP$	1.20e-13	1.18e-13	1.18e-13	0.0
ϕ(E >1.0 MeV) [n/cm^2-s]		4.60e+10	4.57e+10	-0.7

Ex-Vessel (χ^2/Degree of Freedom = 0.44)

Reaction	Reaction Rate [rps/atom]			Adjustment % of Calc.
	Measured	Calculated	Adjusted	
$^{63}Cu(n,\alpha)^{60}Co$	4.01e-19	3.88e-19	4.09e-19	5.4
$^{46}Ti(n,p)^{46}Sc$	6.17e-18	5.54e-18	5.82e-18	5.1
$^{54}Fe(n,p)^{54}Mn$	3.59e-17	3.53e-17	3.67e-17	4.0
$^{58}Ni(n,p)^{58}Co$	5.29e-17	5.32e-17	5.49e-17	3.2
$^{238}U(n,p)FP$	2.72e-16	2.44e-16	2.50e-16	2.5
ϕ(E >1.0 MeV) [n/cm^2-s]		9.65e+08	9.80e+08	1.6

Table 3-11
Summary of Least Squares Adjustment Results for the H. B. Robinson Benchmark

Location	ϕ(E > 1.0 MeV) [n/cm2-s]		A/C
	Calculated	Adjusted	
In-Vessel	4.60e+10 (15%)	4.57e+10 (5%)	0.99
Ex-Vessel	9.65e+08 (15%)	9.80e+08 (7%)	1.02

Note: Numbers in parentheses represent one standard deviation.

Table 3-12
M/C Comparisons for the H. B. Robinson Benchmark

Comparisons Before Adjustment

Reaction	M/C	
	In-Vessel	Ex-Vessel
$^{63}Cu(n,\alpha)^{60}Co$	1.03	1.03
$^{46}Ti(n,p)^{46}Sc$	1.07	1.11
$^{54}Fe(n,p)^{54}Mn$	1.01	1.02
$^{58}Ni(n,p)^{58}Co$	0.95	0.99
$^{238}U(n,p)FP$	1.07	1.11
$^{237}Np(n,p)FP$	1.02	
Average	1.03	1.03
% Standard Deviation	4.4	6.5

Comparisons After Adjustment

Reaction	M/C	
	In-Vessel	Ex-Vessel
$^{63}Cu(n,\alpha)^{60}Co$	1.00	0.98
$^{46}Ti(n,p)^{46}Sc$	1.03	1.06
$^{54}Fe(n,p)^{54}Mn$	1.00	0.98
$^{58}Ni(n,p)^{58}Co$	0.96	0.96
$^{238}U(n,p)FP$	1.07	1.09
$^{237}Np(n,p)FP$	1.02	
Average	1.01	1.01
% Standard Deviation	3.6	5.0

4 FERRET SENSITIVITY STUDIES

The information discussed in this section provides an understanding of how the composition of the multiple foil sensor sets and the input values for the uncertainties in the calculated neutron spectrum and measured reaction rates affect the results of the least squares analysis in terms of both the magnitude and uncertainty of the adjusted spectrum.

The threshold foils comprising typical LWR sensor sets respond to different portions of the neutron energy spectrum. These multiple foil measurements are a set of partial measurements of the flux or fluence rather than a group of complete and independent determinations. Of particular interest for weighting and averaging threshold detector measurements is the spectrum coverage of the individual foils, which recognizes that such measurements do not form an equivalent observation set; therefore, they are not easily matched to the principle of maximum likelihood.

This response is shown in Figure 4-1 and Figure 4-2 for the neutron spectra characteristic of an in-vessel surveillance capsule location and an ex-vessel dosimetry location. The graphical representations shown in Figure 4-1 and Figure 4-2 provide response profiles for the $^{63}Cu(n,\alpha)$, $^{54}Fe(n,p)$, $^{238}U(n,f)$, and $^{237}Np(n,f)$ threshold reactions, as well as for the neutron flux ($E > 1.0$ MeV). The $^{46}Ti(n,p)$ and $^{58}Ni(n,p)$ reactions exhibit behavior similar to the $^{63}Cu(n,\alpha)$, $^{54}Fe(n,p)$ reactions, respectively.

From Figure 4-1 and Figure 4-2, it is evident that the response of the higher threshold reactions exhibits significantly different behavior than does the neutron flux ($E > 1.0$ MeV); the fission monitor response shows a better match to the spectral behavior of the neutron flux. This behavior suggests that in order to validate a calculation of the neutron flux ($E > 1.0$ MeV), significant spectral weighting of measured reaction rates should be included in the comparisons. The least squares approach allows this spectral weighting to be included in a rigorous manner. The data from Figure 4-1 and Figure 4-2 also indicate that the makeup of the foil set could affect the final results of the dosimetry comparisons.

4.1 COMPOSITION OF THE MULTIPLE FOIL SENSOR SET

To assess the effect of the makeup of the sensor set on the the least squares adjustment final solution, a parametric study was performed for a typical LWR dosimetry data set. In the parametric study, the calculated neutron spectrum and uncertainty was held constant along with the uncertainties associated with the measured reaction rates. The base case consisted of an evaluation, including the threshold reactions, whereas the variations in the analysis were accomplished by deleting foil reactions individually and in combination. The 11 cases analyzed in the parametric study are summarized as follows:

Case	Foils Included in the FERRET Analysis					
	Cu	Ti	Fe	Ni	^{238}U	^{237}Np
1	X	X	X	X	X	X
2	X		X	X	X	X
3	X		X		X	X
4			X		X	X
5			X			X
6			X		X	
7					X	X
8					X	
9			X			
10						
11	X					

The results of the least squares evaluations for each of these 11 cases are as follows:

Case	ϕ(E > 1.0 MeV) [n/cm^2-s]		A/C	% Diff From Case 1
	Calculated	Adjusted		
1	4.45e+10 (15%)	4.64e+10 (6%)	1.04	
2	4.45e+10 (15%)	4.64e+10 (6%)	1.04	0.0
3	4.45e+10 (15%)	4.75e+10 (6%)	1.07	2.4
4	4.45e+10 (15%)	4.76e+10 (6%)	1.07	2.6
5	4.45e+10 (15%)	4.69e+10 (7%)	1.05	1.1
6	4.45e+10 (15%)	4.78e+10 (7%)	1.07	3.0
7	4.45e+10 (15%)	4.79e+10 (8%)	1.08	3.2
8	4.45e+10 (15%)	4.60e+10 (12%)	1.03	-0.9
9	4.45e+10 (15%)	4.84e+10 (9%)	1.09	4.3
10	4.45e+10 (15%)	4.69e+10 (9%)	1.05	1.1
11	4.45e+10 (15%)	4.80e+10 (12%)	1.08	3.4

Note: Numbers in parentheses represent one standard deviation.

This data tabulation shows that in terms of the magnitude of the adjusted solution the results for all cases are within the uncertainty of the base case (Case 1). However, the uncertainty in the adjusted flux increases as the content of the foil set is reduced with the highest uncertainties occurring when only a single foil is used in conjunction with the transport calculation.

The data in the tabulation further shows that for a minimum uncertainty solution the foil set should consist of at least Fe, U, and Np foils (Case 4). The addition of Cu, Ti, and Ni do not enhance the capability of the foil set. This is because the very high threshold of the $^{63}Cu(n,\alpha)$ and $^{46}Ti(n,p)$ reactions places their response well above the important energy range for the neutron flux (E > 1.0 MeV) and the

^{58}Ni(n,p) response is so similar to ^{54}Fe(n,p) that the reaction is redundant. Further reductions in the foil set from the Fe, ^{238}U, ^{237}Np package results in an increased uncertainty in the adjusted flux.

4.2 INPUT UNCERTAINTIES

A second sensitivity study was completed to evaluate the effect of the input uncertainties in the measured reaction rates and the calculated neutron flux on the adjusted solution and the final uncertainties determined by the FERRET least squares procedure. In performing this sensitivity study, the following uncertainty matrix was evaluated for the reaction rates and calculated spectra:

Reaction Rate Uncertainties

Reaction Type	Uncertainty Category		
	High	Medium	Low
Non-Fission	10%	5%	2.5%
Fission	20%	10%	5.0%

Neutron Spectrum Uncertainties

Reaction Type	Uncertainty Category		
	High	Medium	Low
Normalization	30%	20%	10%
Spectrum Groups 1-53	30%	20%	10%
Spectrum Groups 28-48	50%	25%	10%
Spectrum Groups 48-53	100%	50%	25%

In this sensitivity study, the "High" category would tend to overstate achievable uncertainties, the "Medium" category would represent a routinely achievable case, and the "Low" category would be equivalent to values achievable in the laboratory or benchmark environment.

The results of the input uncertainty sensitivity study are summarized as follows:

Adjusted ϕ(E > 1.0 MeV) and % Standard Deviation

Flux Spectrum Uncertainty	Reaction Rate Uncertainty		
	High	Medium	Low
High	2.05e+10 (16%)	2.11e+10 (14%)	2.14e+10 (13%)
Medium	1.99e+10 (12%)	2.04e+10 (10%)	2.10e+10 (9%)
Low	2.00e+10 (7%)	1.98e+10 (6%)	2.03e+10 (5%)

Considering the "Medium"-"Medium" case as the baseline, the magnitude of the adjusted flux varies by less than 5% for all of the cases evaluated, indicating that the magnitude of the adjusted flux is dependent primarily on the magnitude of the inputs, rather than on the input uncertainties. However, the associated uncertainty varies in a predictable trend from 5% for the "Low"-"Low" case to 16% for the "High"-"High".

The indications from this sensitivity study indicate that the FERRET least squares algorithm is operating as anticipated.

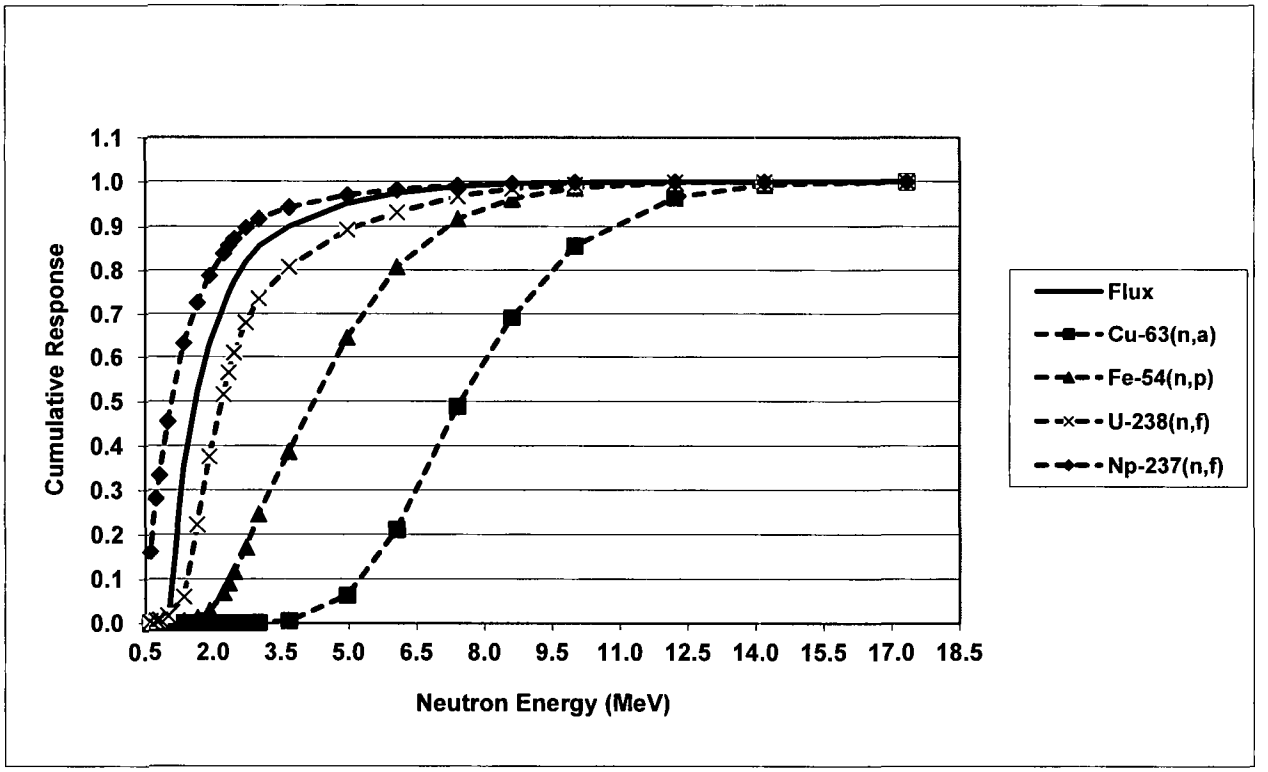

Figure 4-1 Cumulative Sensor Response as a Function of Neutron Energy In-Vessel Surveillance Capsule Location

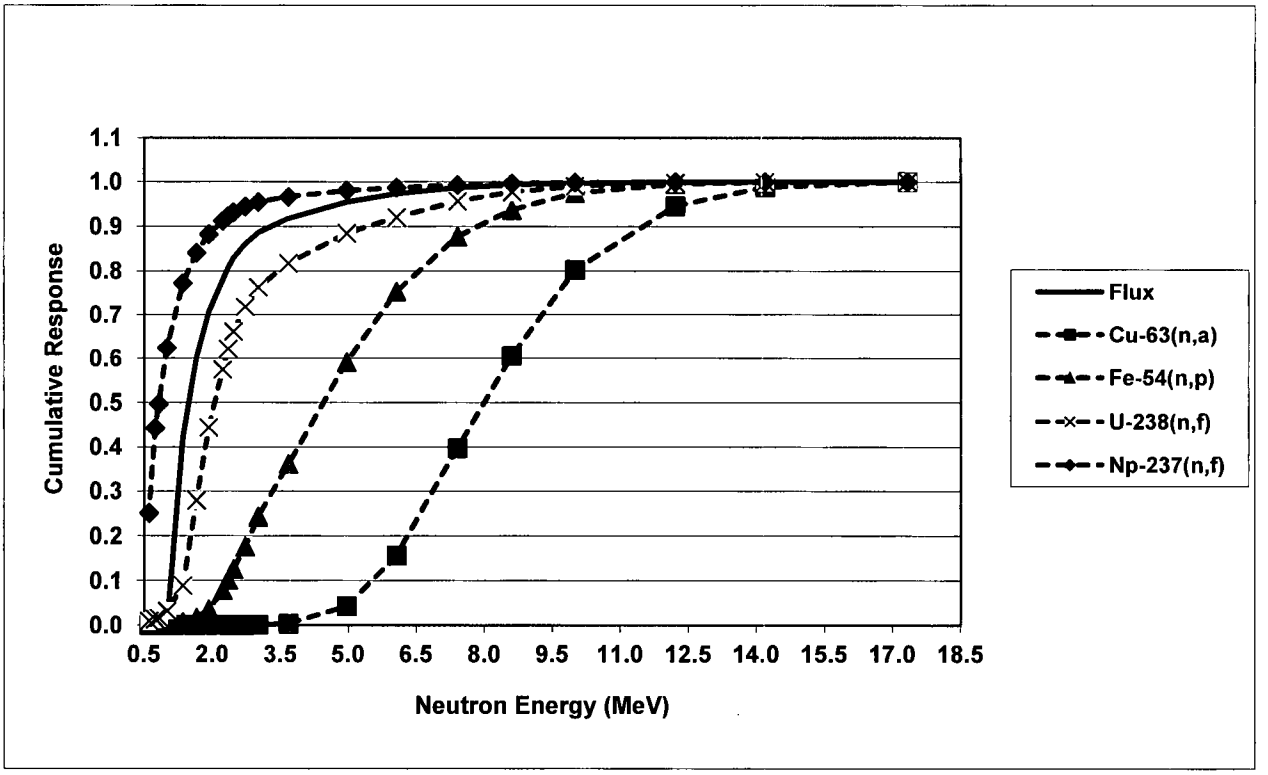

Figure 4-2 Cumulative Sensor Response as a Function of Neutron Energy Ex-Vessel Dosimetry Location

4.3 OPERATING POWER REACTOR COMPARISONS

In addition to the sensitivity studies described above, the transport methodology and the least squares dosimetry evaluations have been extensively compared with data from operating power reactors. These comparisons are intended to provide support for the validation of the transport calculation itself as well as validation for the uncertainties assigned to the results of those calculations.

One concern that operating power plants have raised in regard to measurement/calculation comparisons is that the uncertainties in the positioning of the dosimetry within the reactor could lead to large uncertainties in the measurement/calculation database that would tend to reduce the value of these comparisons. The data comparisons provided in this section are intended to demonstrate that the dosimetry locations within operating power reactors are known within the manufacturing tolerances and that, when calculations and dosimetry processing are completed on a consistent basis, the uncertainties in the measurement/calculation database are less than those associated with the stand alone calculation.

In Section 2.3 of this report, it was noted that the combination of benchmarking comparisons and analytical sensitivity studies resulted in an evaluated uncertainty of 13% (1σ) in the calculation of neutron flux or fluence ($E > 1.0$ MeV). Based on the analytical sensitivity studies using allowable manufacturing tolerances for the reactor components as limits, the component of the uncertainty in measurement/calculation comparisons due to miss-positioning of surveillance capsule dosimetry is in the range of 4-5% (1σ).

To demonstrate the validity of these uncertainty assessments, comparisons using the methodologies described in Section 2 of this report were applied to a large measurement database consisting of 104 surveillance capsule dosimetry sets withdrawn from 29 reactors having Westinghouse or Combustion Engineering as the Original Equipment Manufacturer (OEM) of the NSSS. The database includes surveillance capsules attached to the pressure vessel wall, capsules mounted on the external surfaces of thermal shields or neutron pads, and accelerated capsules mounted on the core barrel. The irradiation times included in the database range from 1 to greater than 20 fuel cycles. The number of capsules withdrawn from individual reactors ranges from two to six. The overall database includes five basic Westinghouse internals configurations and two Combustion Engineering internals designs.

In Table 4-1, the comparisons of the adjusted results with the original calculations of the neutron flux ($E > 1.0$ MeV) are provided as [adjusted]/[calculated] (A/C) ratios for each of the 104 surveillance capsule dosimetry sets included in the database. Also included in the tabulation are average A/C values for the 29 individual reactors and for the overall database. From the data listed in Table 4-1, the overall database average A/C is 0.99 with an associated standard deviation of 7%. This data shows that the stand alone transport calculations are essentially unbiased. Further, the 7% standard deviation associated with the A/C database is approximately half of the 13% uncertainty assigned to the calculation alone. It is evident from this database that lack of knowledge of dosimeter positioning does not introduce large scatter and correspondingly high uncertainty into the comparisons of dosimetry results with calculations.

Although the data comparisons listed in Table 4-1 compare the results of the least squares adjustment with the original calculated neutron flux ($E > 1.0$ MeV), similar conclusions regarding the effects of dosimetry positioning can be drawn from a comparison of [measurement]/[calculation] (M/C) ratios for individual foil reactions. These comparison applicable to the 104 capsule database are listed in Table 4-2 along with

the previously discussed A/C results from the adjustment analysis. From Table 4-2, none of the comparisons for the individual foil reactions show any excessive scatter that could be attributed to a large uncertainty in the dosimeter positioning.

A key factor in completing the comparisons of calculation and measurement is that, for all data points, both the transport calculations and the dosimetry evaluations must be done using the same methods, cross-sections, and basic nuclear data. Use of older published data based on different methods and assumptions will lead to distortions in the database. This could be due to one or more of the following:

1. Changes in treatment of the core source (conservative vs. best estimate)

2. Changes in transport cross-sections (ENDF/B-IV vs. ENDF/B-VI)

3. Changes in dosimetry cross-sections (ENDF/B-IV vs. ENDF/B-VI)

4. Changes in dosimetry evaluation methods (spectrum averaged cross-sections vs. least squares adjustment)

These artificial distortions could introduce data scatter that would lead to a misinterpretation of the validity of the database.

Consider the following example for Reactor 15 from Table 4-1:

The Reactor 15 database consists of 5 surveillance capsule withdrawals during the 20 year interval between 1985 and 2004. The original documentation of each of those capsule analyses was based on the methodology and basic nuclear data accepted at the time of the evaluations. These are summarized as follows:

1. Completed in 1985.
   Spectrum averaged cross-section dosimetry evaluation.
   Design basis power distribution, intended to be conservative.
   ENDF/B-IV transport cross-sections (SAILOR).
   ENDF/B-V dosimetry cross-sections.

2. Completed in 1988.
   Spectrum averaged cross-section dosimetry evaluation
   Plant specific power distribution, intended to be best estimate.
   ENDF/B-IV transport cross-sections (SAILOR).
   Axial peaking based on core power distribution.
   ENDF/B-V dosimetry cross-sections.

3. Completed in 1991.
   Least squares dosimetry evaluation.
   Plant specific power distribution, intended to be best estimate.
   ENDF/B-IV transport calculations (SAILOR).

Axial peaking based on core power distribution.
ENDF/B-V dosimetry cross-sections.

4. Completed in 1998.
Least squares dosimetry evaluation.
Plant specific power distribution, intended to be best estimate.
ENDF/B-VI transport cross-sections (BUGLE-96).
Axial peaking based on core power distribution.
ENDF/B-VI dosimetry cross-sections (SNLRML).

5. Completed in 2004.
Least squares dosimetry evaluation.
Plant specific power distribution, intended to be best estimate.
ENDF/B-VI transport cross-sections (BUGLE-96).
Axial peaking based on 3D synthesis.
ENDF/B-VI dosimetry cross-sections (SNLRML).

The methodology used for the latest evaluations for Reactor 15 is identical to those described in Section 2 of this report.

The following tabulation provides a comparison of the M/C or A/C ratios taken from the original reports for each of the capsule withdrawals from Reactor 15 with the latest A/C comparisons based on the methodology described in Section 2.

Capsule	Original M/C or A/C	Latest A/C
1	0.86	0.93
2	1.03	0.94
3	1.11	0.96
4	0.98	0.98
5	0.95	0.95
Average	0.99	0.95
% std dev	9.4	2.0

This comparison shows that the use of consistent methodologies for calculation and dosimetry evaluation reduces the standard deviation in the database by almost a factor of five. This clearly demonstrates that changing methodologies can introduce significant scatter in the database and shows the importance of re-evaluating dosimetry from previously withdrawn capsules each time a new surveillance capsule from a given reactor is analyzed.

Table 4-1
Database Comparison for 104 In-Vessel Dosimetry Sets from 29 Reactors

Reactor	A/C Ratio – Neutron Flux (E > 1.0 MeV)							
	Capsule 1	Capsule 2	Capsule 3	Capsule 4	Capsule 5	Capsule 6	Average	% std
1	1.10	1.01	1.05	0.93			1.02	7.0
2	1.03	0.96	0.97	0.92			0.97	4.7
3	1.00	0.89	0.86				0.92	8.0
4	1.03	0.94	1.05	1.03			1.01	4.9
5	1.08	0.99	0.94				1.00	7.1
6	1.01	0.99	0.97	0.95			0.98	2.6
7	0.94	1.06	1.06				1.02	6.8
8	1.01	1.02	1.02	1.01			1.02	0.6
9	0.99	1.04	1.01	0.93			0.99	4.7
10	0.85	1.03	1.04	0.97			0.97	8.7
11	1.16	0.92					1.04	16.3
12	0.95	1.02	0.91	0.99			0.97	4.9
13	1.01	0.99	0.93	0.84	0.96		0.95	7.0
14	0.97	0.98	0.95				0.97	1.6
15	0.93	0.94	0.96	0.98	0.95		0.95	2.0
16	0.94	0.97	0.93	0.81	0.88		0.91	6.9
17	0.94	0.86	0.89	1.04	0.85		0.92	8.5
18	0.94	0.91					0.93	2.3
19	1.06	0.94	0.88	0.99			0.97	7.9
20	0.98	0.96	1.01	1.04			1.00	3.5
21	1.07	1.02	1.14	1.04			1.07	4.9
22	1.04	1.07					1.06	2.0
23	0.99	1.01					1.00	1.4
24	1.06	1.01	1.07				1.05	3.1
25	1.05	0.95	1.06				1.02	6.0
26	1.13	1.05	0.97				1.05	7.6
27	0.99	0.96	1.01	0.98	1.08	1.09	1.02	5.3
28	1.12	0.94	0.99				1.02	9.1
29	0.93	1.14					1.04	14.3
Average							**0.99**	**7.0**

Table 4-2
Summary Comparison for Individual Foil Reactions

Reaction	Database Average M/C or A/C	% std dev
$^{63}Cu(n,\alpha)^{60}Co$	1.08	7.2
$^{54}Fe(n,p)^{54}Mn$	0.98	7.9
$^{58}Ni(n,p)^{58}Co$	0.98	7.9
$^{238}U(n,p)FP$	1.01	11.4
$^{237}Np(n,p)FP$	1.04	11.7
$\phi(E > 1.0\ MeV)$	0.99	7.0

5 SUMMARY AND CONCLUSIONS

In this report, the use of the FERRET adjustment code for the least squares evaluation of LWR surveillance dosimetry has been described and benchmarked. The ability of the least squares procedure to combine calculations with available measurements to determine the best estimate spectrum with reduced uncertainties at the measurement locations has been demonstrated by benchmark comparisons in the NIST ^{235}U and ^{237}Np standard fission fields, the PCA simulator benchmark, and the H. B. Robinson power reactor benchmark.

The importance of the key input parameters (Neutron spectrum, measured reaction rates, and dosimetry cross-sections) and their associated uncertainties have been discussed and the values used in the Westinghouse least squares procedure have been described and justified. The sensitivity of the adjustment procedure to the makeup of the foil set and the input uncertainties in the calculated spectrum and the measured reaction rates has been provided.

The conclusions from these studies are as follows:

1. The FERRET code operates as intended as a least squares adjustment code for reactor dosimetry analyses.

2. The input parameters (calculated neutron spectrum, measured reaction rates, and dosimetry reaction cross-sections) and their associated uncertainties are appropriate for use in LWR dosimetry evaluations.

3. The adjusted neutron flux (E > 1.0 MeV) from the FERRET evaluations can be used to develop a database for use in validating plant specific neutron transport calculations for LWR pressure vessels. This adjustment process provides a rigorous spectrum weighting of individual reaction rate M/C comparisons.

The comparison database developed from the least squares evaluation of the dosimetry sets can be used along with the guidance in Regulatory Guide 1.190 to validate neutron transport calculations and to determine any calculational biases that may be present.

6 REFERENCES

1. Code of Federal Regulations Title 10 Part 50, "Domestic Licensing of Production and Utilization Facilities," Appendix G, "Fracture Toughness Requirements" and Appendix H, "Reactor Vessel Material Surveillance Requirements."

2. Code of Federal Regulations Title 10 Part 50.61, "Fracture Toughness Requirements for Protection Against Pressurized Thermal Shock Events."

3. Regulatory Guide 1.190, "Calculational and Dosimetry Methods for Determining Pressure Vessel Neutron Fluence," U.S. Nuclear Regulatory Commission, Office of Nuclear Regulatory Research, March 2001.

4. ASTM Designation E944, 2013, "Standard Guide for Application of Neutron Spectrum Adjustment Methods in Reactor Surveillance," ASTM International, West Conshohocken, PA, 2013, DOI: 10.1520/E0944-13, www.astm.org.

5. RSIC Code Package PSR-145, "FERRET Least Squares Solution to Nuclear Data and Reactor Physics Problems," Radiation Shielding Information Center, Oak Ridge National Laboratory (ORNL), January 1980.

6. F. Schmittroth, "FERRET Data Analysis Code," HEDL-TME-79-40, Hanford Engineering Development Laboratory, September 1979.

7. RSIC Code Package PSR-277, "LEPRICON PWR Pressure Vessel Surveillance Dosimetry Analysis System," Radiation Shielding Information Center, Oak Ridge National Laboratory (ORNL), June 1995.

8. RSIC Code Package PSR-113, "STAY'SL Least Squares Dosimetry Unfolding Code System," Radiation Shielding Information Center, Oak Ridge National Laboratory (ORNL), December 1991.

9. RSIC Code Package PSR-233, "LSL-M2 Least Squares Logarithmic Adjustment of Neutron Spectra," Radiation Shielding Information Center, Oak Ridge National Laboratory (ORNL), February 1991.

10. RSICC Computer Code Collection CCC-650, "DOORS 3.1, One- Two- and Three Dimensional Discrete Ordinates Neutron/Photon Transport Code System," Radiation Safety Information Computational Center, Oak Ridge National Laboratory (ORNL), August 1996.

11. RSIC Data Library Collection DLC-185, "BUGLE-96, Coupled 47 Neutron, 20 Gamma Ray Group Cross-Section Library Derived from ENDF/B-VI for LWR Shielding and Pressure Vessel Dosimetry Applications," Radiation Shielding Information Center, Oak Ridge National Laboratory (ORNL), March 1996.

12. R. L. Simons, et. al, "Re-Evaluation of the Dosimetry for Reactor Pressure Vessel Surveillance Capsules," in NUREG/CP-0029, "Proceedings of the Fourth ASTM-EURATOM Symposium on Reactor Dosimetry," F. B. K. Kam, Editor, July 1982.

13. W. N. McElroy, et. al, "LWR PV Surveillance Dosimetry Improvement Program: PCA Experiments and Blind Test," NUREG/CR-1861, July 1981.

14. Regulatory Guide 1.99, Revision 2, "Radiation Embrittlement of Reactor Vessel Materials," U. S. Nuclear Regulatory Commission, Office of Nuclear Regulatory Research, May 1988.

15. G. L. Guthrie, "Uncertainty Considerations in Development and Application of Charpy Trend Curve Formulas," in REACTOR DOSIMETRY Dosimetry Methods for Fuels, Cladding, and Structural Materials, Proceedings of the Fifth ASTM-Euratom Symposium on Reactor Dosimetry, GKSS Research Centre, Geesthact, F. R. G., J. P Genthon and H Rottger, Editors, D. Reidel Publishing Company, 1985.

16. G. L. Guthrie, "Charpy Trend Curve Development Based on PWR Surveillance Data," in NUREG/CP-0048 Proceedings of the U. S. Nuclear Regulatory Commission Eleventh Water Reactor Safety Research Information Meeting, Volume 4 – Materials Engineering Research," U. S. Nuclear Regulatory Commission, Office of Nuclear Regulatory Research, January 1984.

17. G. L. Guthrie, "Charpy Trend Curves Based on 177 PWR Data Points," NUREG/CR-3391, Volume 2, LWR-PV-SDIP Quarterly Progress Report, April 1983.

18. ASTM Designation E1018, 2009, "Standard Guide for Application of ASTM Evaluated Cross-Section Data File," ASTM International, West Conshohocken, PA, 2009, DOI: 10.1520/E1018-09, www.astm.org.

19. ASTM Designation E261, 2010, "Standard Practice for Determining Neutron Fluence, Fluence Rate, and Spectra by Radioactivation Techniques," ASTM International, West Conshohocken, PA, 2010, DOI: 10.1520/E0261-10, www.astm.org.

20. W. N. McElroy, et. al, "LWR Pressure Vessel Surveillance Dosimetry Improvement Program: PCA Experiments, Blind Test, and Physics-Dosimetry Support for the PSF Experiments," NUREG/CR-3318, September 1984.

21. I. Remec and F. B. K. Kam, "Pool Critical Assembly Pressure Vessel Facility Benchmark," NUREG/CR-6454, July 1997.

22. A. K. McCracken, "Few Channel Unfolding in Shielding – The SENSAK Code," in Proceedings of the 3rd ASTM-EURATOM Symposium on Reactor Dosimetry, Ispra, Italy, October 1-5, 1979, EUR 6813, Commission of the European Communities, Vol. II, P. 732, 1980.

23. RSIC Data Library Collection DLC-178, "SNLRML Recommended Dosimetry Cross Section Compendium," Radiation Shielding Information Center, Oak Ridge National Laboratory, July 1994.

24. N. P. Kocherov, et. al, "International Reactor Dosimetry File (IRDF-90)," International Atomic Energy Agency, Nuclear Data Section, IAEA-NDS-141, Rev. 0, August 1990.

25. I. Remec and F. B. K. Kam, "H. B. Robinson Pressure Vessel Benchmark," NUREG/CR-6453 (ORNL/TM-13204), February 1998.

26. J. D. Andrachek, et. al, "Methodology Used to Develop Cold Overpressure Mitigating System Setpoints and RCS Heatup and Cooldown Limit Curves," WCAP-14040-A, Revision 4, May 2004.

27. B. Petrovic, A. Haghighat, "Analysis of Inherent Oscillations in S_N Solutions of the Neutron Transport Equation," Nuclear Science and Engineering, Vol. 124, pp. 31-62, 1996.

28. G. Sjoden, A. Haghighat, "The Exponential Directional Weighted (EDW) Differencing Scheme in 3-D Cartesian Geometry," *Proc. Joint Int. Conf. Mathematical Methods and Supercomputing for Nuclear Applications*, Saratoga Springs, New York, October 5–9, 1997, Vol. II, p. 1267 (1997).

29. G. Fischer, "Analysis of the Pool Critical Assembly Benchmark Using RAPTOR-M3G, a Parallel Deterministic Radiation Transport Code," *Proc. PHYSOR 2010*, Pittsburgh, PA, May 9–14, 2010, Vol. I, p. 506 (2010).

30. RSICC Data Library Collection DLC-245, "BUGLE-B7/VITAMIN-B7, Broad-Group and Fine-Group and Coupled Neutron/Gamma Cross-Section Libraries Derived from ENDF/B-VII.0 Nuclear Data," Radiation Safety Information Computational Center, Oak Ridge National Laboratory (ORNL), October 2011.

APPENDIX A PARALLEL-PROCESSING NEUTRON TRANSPORT CALCULATIONS WITH RAPTOR-M3G

Neutron transport calculations and their uncertainties are discussed in detail in Section 2.3 of this report.

The numerical solution of the Linearized Boltzmann Equation via the Discrete Ordinates S_N method requires extensive computational resources for large three-dimensional neutron and gamma-ray transport applications due to the concurrent discretization of the angular, spatial, and energy domains. The discretization of the phase-space of the transport equation imposes large memory and processing requirements which can easily overwhelm the capabilities of single processor workstations. Using the previous generation of discrete ordinates neutron transport codes, such as DORT and TORT[10], analysts frequently encounter limitations in the amount of detail they can represent in their models. This often necessitates overly-conservative simplifying assumptions.

Recent years have seen the widespread application of parallel processing techniques to solve problems in almost every area of scientific computing. This shift has been driven by the commoditization of powerful computer hardware and the development of high-speed, low-latency networking technologies. Parallel processing techniques allow a given problem to be solved more quickly, and they allow a large problem to be distributed across the memory of multiple computers. This enables the solution of significantly larger problems, and provides results on a timescale conducive to production engineering applications.

To take advantage of these benefits, Westinghouse has developed RAPTOR-M3G, a three-dimensional parallel discrete ordinates (S_N) radiation transport code. The methodology employed by RAPTOR-M3G is identical to the methodology employed by the TORT code, with a number of evolutionary solution enhancements resulting from the last two decades of research[27, 28]. RAPTOR-M3G has been designed from its inception as a parallel processing code, and adheres to modern best practices of software development. It has been rigorously tested against the TORT code[10] and benchmarked on an extensive set of academic and real-world problems.

The results presented in this Appendix focus exclusively on comparisons between measurements and calculations, with no consideration given to any least squares adjustments.

A.1 PCA SIMULATOR BENCHMARK

The configuration of the PCA Simulator benchmark is discussed in detail in Section 3.2 of this report.

In this Appendix, the PCA benchmark has been re-analyzed on a modern computing platform with TORT and RAPTOR-M3G. As part of this effort, the original problem has been further refined to take advantage of the increased computing capabilities available at the present time. The current PCA problem is modeled on a 67 × 139 × 102 Cartesian mesh grid. This is sufficient to achieve a maximum mesh cell spacing of approximately 1.0 cm in each dimension across the entire problem. Angular quadrature is modeled with an S_8 level-symmetric quadrature set, and anisotropic scattering is treated with a P_3 Legendre expansion. (Note that this problem has also been analyzed with RAPTOR-M3G using S_{16} quadrature and P_5 Legendre expansion [29]. The present purpose is to perform a comparison with TORT. Therefore, the size of the problem has been constrained such that it is readily solvable with TORT.)

The transport cross-section set was constructed from the BUGLE-96 library[11], and dosimetry reaction rate cross-sections are taken from the SNLRML library[23]. The PCA problem was analyzed in both RAPTOR-M3G and TORT with the theta-weighted differencing scheme[10], which corresponds to the MODE = 0 input option of the TORT code. The value of theta selected for this problem is 0.9. Results from TORT are presented in Table A-1, and results from RAPTOR-M3G are presented in Table A-2.

Table A-1 and Table A-2 demonstrate that RAPTOR-M3G and TORT produce identical results within the precision reported in the tables. Table A-3 compares the 47-group neutron spectrum (in BUGLE-96 group structure) generated by RAPTOR-M3G and TORT for measurement location A7. The results for each individual group agree to within 1%, and most groups are within or very close to the problem convergence criteria of 0.1%.

Table A-1

M/C Comparisons for the PCA 12/13 Blind Test Experiment Performed with TORT

	M/C Ratio for Dosimetry Position Noted						
	A1	**A2**	**A3**	**A4**	**A5**	**A6**	**A7**
$^{27}Al(n,\alpha)^{24}Na$ (Cd)	0.99	1.00	0.95	0.95	0.96	0.98	
$^{58}Ni(n,p)^{58}Co$ (Cd)	1.03	1.03	0.99	1.00	1.01	0.97	
$^{115}In(n,n')^{115m}In$ (Cd)	1.03	1.03	0.97	0.97	0.99	1.00	1.06
$^{103}Rh(n,n')^{103m}Rh$ (Cd)	1.01	0.98	0.98	0.98	1.04	1.06	1.07
$^{238}U(n,f)FP$ (Cd)			0.92	1.01	1.03	1.06	1.06
$^{237}Np(n,f)FP$ (Cd)			1.07	1.00	0.99	1.03	0.98
Average	1.02	1.01	0.98	0.99	1.00	1.02	1.04
% std dev	1.9	2.4	5.2	2.3	2.9	3.9	4.0

Table A-2

M/C Comparisons for the PCA 12/13 Blind Test Experiment Performed with RAPTOR-M3G

	M/C Ratio for Dosimetry Position Noted						
	A1	**A2**	**A3**	**A4**	**A5**	**A6**	**A7**
$^{27}Al(n,\alpha)^{24}Na$ (Cd)	0.99	1.00	0.95	0.95	0.96	0.98	
$^{58}Ni(n,p)^{58}Co$ (Cd)	1.03	1.03	0.99	1.00	1.01	0.97	
$^{115}In(n,n')^{115m}In$ (Cd)	1.03	1.03	0.97	0.97	0.99	1.00	1.06
$^{103}Rh(n,n')^{103m}Rh$ (Cd)	1.01	0.98	0.98	0.98	1.04	1.06	1.07
$^{238}U(n,f)FP$ (Cd)			0.92	1.01	1.03	1.06	1.06
$^{237}Np(n,f)FP$ (Cd)			1.07	1.00	0.99	1.03	0.98
Average	1.02	1.01	0.98	0.99	1.00	1.02	1.04
% std dev	1.9	2.4	5.2	2.3	2.9	3.9	4.0

Table A-3

Calculated 47-Group Neutron Spectra at Measurement Location A7 Generated by RAPTOR-M3G and TORT

Group	TORT Flux (n/cm^2-s)	RAPTOR-M3G Flux (n/cm^2-s)	TORT / RAPTOR-M3G Flux Ratio
1	6.437E-13	6.437E-13	1.000
2	1.897E-12	1.897E-12	1.000
3	7.750E-12	7.752E-12	1.000
4	1.417E-11	1.417E-11	1.000
5	2.191E-11	2.191E-11	1.000
6	4.606E-11	4.607E-11	1.000
7	6.415E-11	6.414E-11	1.000
8	1.162E-10	1.162E-10	1.000
9	9.015E-11	9.016E-11	1.000
10	7.094E-11	7.095E-11	1.000
11	8.429E-11	8.433E-11	1.000
12	4.474E-11	4.475E-11	1.000
13	1.406E-11	1.407E-11	0.999
14	7.078E-11	7.079E-11	1.000
15	1.951E-10	1.952E-10	0.999
16	2.739E-10	2.740E-10	1.000
17	4.478E-10	4.479E-10	1.000
18	1.061E-09	1.061E-09	1.000
19	9.782E-10	9.782E-10	1.000
20	3.823E-10	3.823E-10	1.000
21	2.096E-09	2.098E-09	0.999
22	1.615E-09	1.614E-09	1.001
23	1.676E-09	1.677E-09	0.999
24	2.413E-09	2.411E-09	1.001
25	2.183E-09	2.175E-09	1.004
26	2.179E-09	2.167E-09	1.006
27	1.186E-09	1.183E-09	1.003
28	6.800E-10	6.787E-10	1.002
29	1.384E-10	1.384E-10	1.000
30	9.926E-11	9.916E-11	1.001
31	6.510E-10	6.525E-10	0.998
32	3.510E-10	3.516E-10	0.998
33	3.984E-10	3.988E-10	0.999
34	3.748E-10	3.749E-10	1.000
35	4.539E-10	4.538E-10	1.000

Group	TORT Flux (n/cm^2-s)	RAPTOR-M3G Flux (n/cm^2-s)	TORT / RAPTOR-M3G Flux Ratio
36	3.643E-10	3.640E-10	1.001
37	5.927E-10	5.918E-10	1.002
38	2.960E-10	2.956E-10	1.001
39	3.246E-10	3.242E-10	1.001
40	4.231E-10	4.224E-10	1.002
41	5.013E-10	5.003E-10	1.002
42	2.780E-10	2.776E-10	1.001
43	3.386E-10	3.381E-10	1.001
44	2.357E-10	2.354E-10	1.001
45	2.116E-10	2.113E-10	1.001
46	3.557E-10	3.553E-10	1.001
47	6.068E-09	6.053E-09	1.002

A.2 H. B. ROBINSON BENCHMARK

The configuration of the H. B. Robinson benchmark is discussed in detail in Reference 25.

In this appendix, the H. B. Robinson benchmark problem has been reanalyzed with RAPTOR-M3G. The current H. B. Robinson geometry is modeled on a 158 × 136 × 172 cylindrical mesh grid. Angular quadrature is modeled with an S_{12} level-symmetric quadrature set, and anisotropic scattering is treated with a P_5 Legendre expansion. The transport cross-section set was constructed from the BUGLE-96 library[11], and dosimetry reaction rate cross-sections are taken from the SNLRML library[23]. The problem is analyzed with the directional theta-weighted differencing scheme[27].

Results are presented in Table A-4, showing comparisons of the measurement to calculation ratios for each sensor. From Table A-4, note that the averaged M/C ratios for the in-vessel sensors range from 1.03 to 1.20, with an overall average of 1.08 and a 1-σ standard deviation of 5.8%. The M/C ratios for the ex-vessel sensors range from 0.94 to 1.12, with an overall average of 1.01 and a 1-σ standard deviation of 7.5%. The comparisons show that the baseline calculation and the reaction rate measurements are in good agreement for all reactions at all measurement locations.

Note that the results in this appendix made no attempt to address power redistribution effects over the course of the fuel cycle when calculating measured reaction rates at saturation, whereas the results presented in Section 3.3 of this report did consider power redistribution. The differences in the comparisons between measurements and calculations are largely attributable to this phenomenon. See Appendix A of Reference 25 for a detailed discussion.

Table A-4

M/C Comparisons for the H. B. Robinson Benchmark Performed with RAPTOR-M3G

Reaction	M/C Ratio	
	In-Vessel	Ex-Vessel
$^{63}Cu(n,\alpha)^{60}Co$	1.06	0.94
$^{46}Ti(n,p)^{46}Sc$	1.20	1.12
$^{54}Fe(n,p)^{54}Mn$	1.04	0.94
$^{58}Ni(n,p)^{58}Co$	1.08	1.03
$^{238}U(n,p)FP$	1.06	1.04
$^{237}Np(n,p)FP$	1.03	
Average	1.08	1.01
% std dev	5.8	7.5

A.3 EX-VESSEL NEUTRON DOSIMETRY ANALYSIS FROM ULCHIN UNIT 5

Supplementary benchmark data for RAPTOR-M3G have been provided by the Korea Reactor Integrity Surveillance Technology (KRIST) company. The data consists of measurements from the ex-vessel neutron dosimetry set installed in Ulchin Unit 5, a 2815 MWt commercial PWR located in South Korea.

In order to supplement the neutron dosimetry provided by the sensor sets contained in the in-vessel surveillance capsules, the ex-vessel neutron dosimetry program was implemented. Multiple foil sensors were installed at several locations in the annular region located between the reflective insulation and the primary biological shield. These multiple foil sets were designed to provide measured reaction rate data sufficient to characterize the neutron spectra at these measurement locations.

The placement of the individual multiple foil sensors within the reactor cavity is illustrated in Figure A-1. In Figure A-1, a plan view of the azimuthal locations of the four strings of sensor sets is depicted. The ex-vessel neutron dosimetry was installed prior to Cycle 5 and the four strings are located at azimuthal locations of 0°, 7°, 14°, and 45° relative to the core cardinal axis 180° Reactor Vessel (RV). The peak flux location on the reactor vessel is 7° relative to the core cardinal axis.

The multiple foil sensor sets used for the ex-vessel measurements were retained in 3.87 ×1.00 × 0.50-inch rectangular aluminum 6061 capsules such as that shown in Figure A-2. Each capsule included three compartments to hold the neutron sensors. The top compartment (Position 1) was intended to accommodate bare radiometric monitors (RMs), while the two remaining compartments (Positions 2 and 3) were designed to hold cadmium-shielded RMs. The separation between Positions 1 and 2 is such that cadmium shields inserted into Position 2 did not introduce perturbations in the neutron flux in Position 1.

Aluminum 6061 was selected for the dosimeter capsules in order to minimize neutron flux perturbations at the sensor set locations, as well as to limit the radiation levels associated with post-irradiation shipping and handling of the irradiated dosimetry.

The Cycle 5 ex-vessel neutron dosimetry set from Ulchin Unit 5 has been analyzed with RAPTOR-M3G. The Ulchin Unit 5 geometry is modeled on a 147 × 82 × 83 cylindrical mesh grid. Angular quadrature is modeled with an S_8 level-symmetric quadrature set, and anisotropic scattering is treated with a P_3 Legendre expansion. The transport cross-section set was constructed from the BUGLE-96 library[11], and dosimetry reaction rate cross-sections are taken from the SNLRML library[23]. The problem is analyzed with the directional theta-weighted differencing scheme[27].

Results are presented in Table A-5, showing comparisons of the measurement to calculation ratios for each sensor. From Table A-5, note that the averaged M/C ratios range from 0.91 to 1.00, with an overall average of 0.97 and a 1-σ standard deviation of 6.3%. The comparisons show that the baseline calculation and the reaction rate measurements are in good agreement for all reactions at all measurement locations.

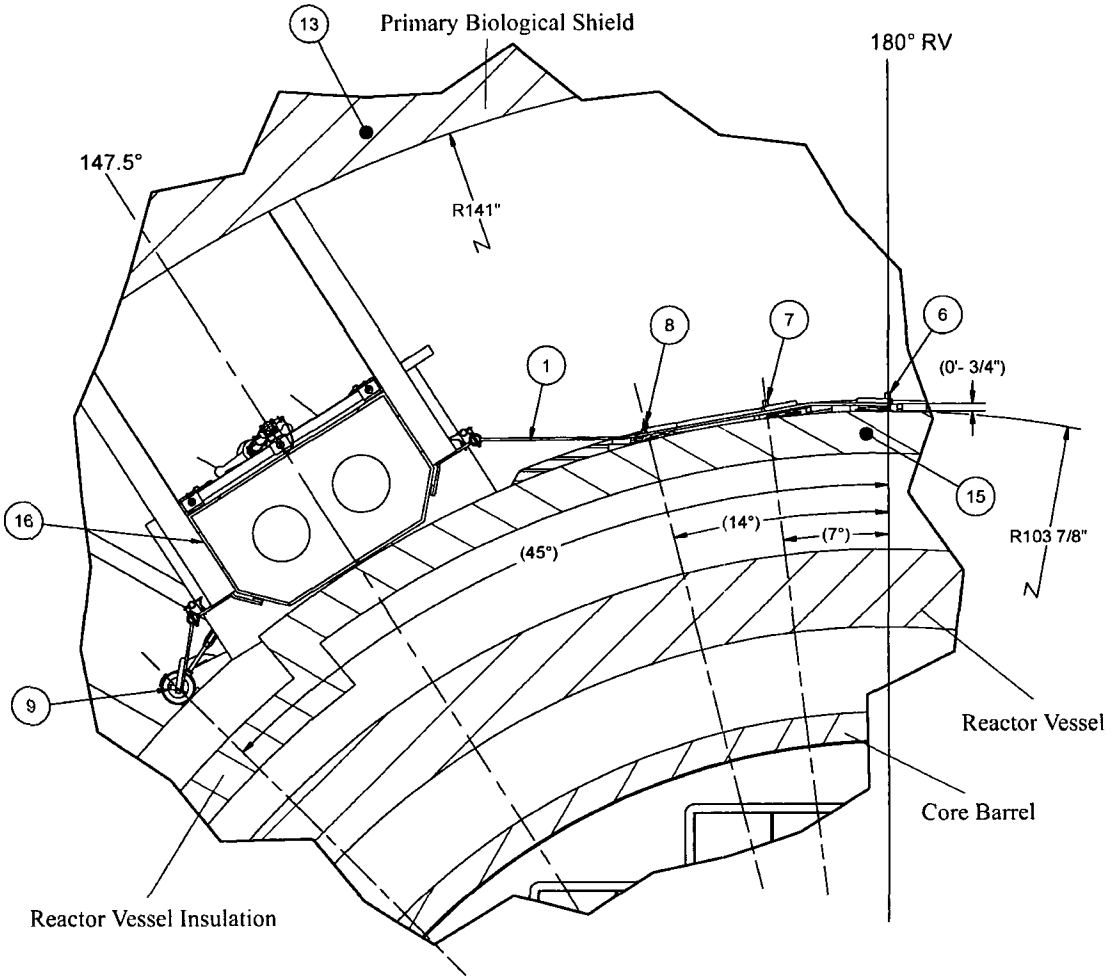

Figure A-1 Plan View of Ex-Vessel Neutron Dosimetry at Ulchin Unit 5

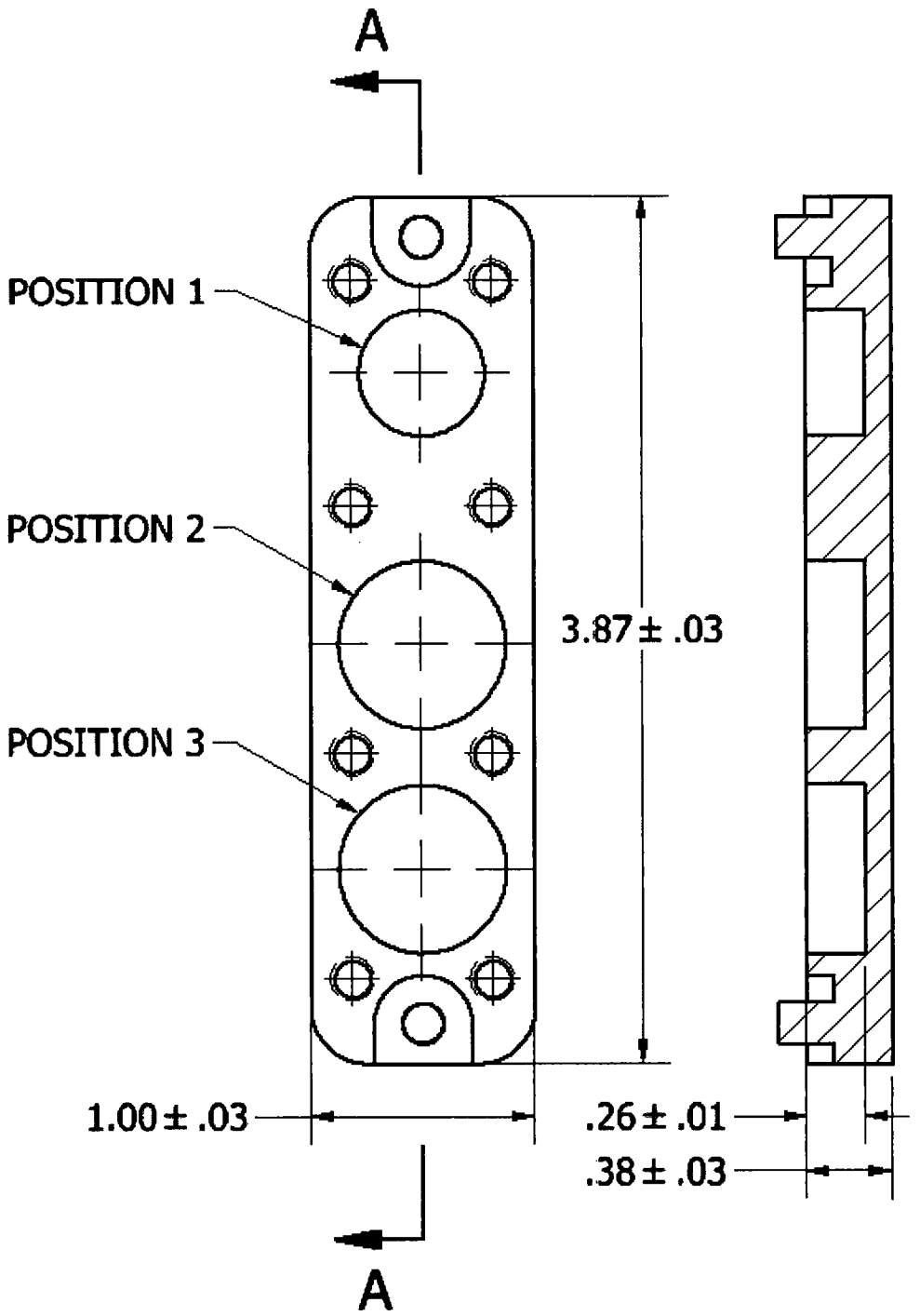

Figure A-2 Irradiation Capsule for Ex-Vessel Multiple Foil Sensor Sets at Ulchin Unit 5 (Dimensions in inches)

Table A-5

M/C Comparisons of Cycle 5 Threshold Reaction Rates in Ulchin Unit 5 Midplane Capsules Performed with RAPTOR-M3G

	M/C Ratio			
	0° Capsule	**7° Capsule**	**14° Capsule**	**45° Capsule**
$^{63}Cu(n,\alpha)^{60}Co$	0.92	0.96	0.99	0.95
$^{46}Ti(n,p)^{46}Sc$	0.95	0.99	1.01	0.97
$^{54}Fe(n,p)^{54}Mn$	0.91	0.86	0.89	0.91
$^{58}Ni(n,p)^{58}Co$	0.91	0.96	0.94	0.94
$^{238}U(n,p)FP$	0.82	1.03	0.93	0.95
$^{237}Np(n,p)FP$	0.80	1.13	1.04	0.93
$^{93}Nb(n,n')^{93m}Nb$	1.07	1.10	1.15	1.02
Average	0.91	1.00	0.99	0.95
% std dev	9.8	9.1	8.7	3.7

Reaction	**Average M/C Ratio**	**% std dev**
$^{63}Cu(n,\alpha)^{60}Co$	0.96	3.0
$^{46}Ti(n,p)^{46}Sc$	0.98	2.6
$^{54}Fe(n,p)^{54}Mn$	0.89	2.6
$^{58}Ni(n,p)^{58}Co$	0.94	2.2
$^{238}U(n,p)FP$	0.93	9.3
$^{237}Np(n,p)FP$	0.98	14.6
$^{93}Nb(n,n')^{93m}Nb$	1.09	5.0
Average	0.97	6.3

A.4 3-LOOP REACTOR VESSEL CLAD SAMPLES ANALYSIS

Small samples (on the order of 200 mg each) were machined from the stainless steel reactor pressure vessel cladding for retrospective dosimetry analysis at a Westinghouse 3-Loop PWR. Samples were taken to measure the axial distribution at the azimuthal neutron flux peak (0°) and azimuthally from 0° to 45° at the core midplane. Two additional measurements were made at 0° and 45° at the axial location of a critical circumferential weld. These samples were collected into a rubber matrix for transport and later separated and counted using several techniques.

In Table A-6 and Table A-7, comparisons of measured to calculation (M/C) ratios are listed for the threshold reactions from a set of Westinghouse 3-Loop reactor pressure vessel clad samples. From Table A-6 and Table A-7, it is noted that for the individual threshold reactions, the average M/C ratio ranges from 0.99 to 1.08 with an overall average of 1.02 and an associated standard deviation of 12.2%. In this case, the overall average was based on an equal weighting of each of the sensor types with no adjustments made to account for the spectral coverage of the individual sensors.

Table A-6

Comparison of Measured and Calculated Threshold Reaction Rates for Westinghouse 3-Loop Pressure Vessel Clad Samples

Azimuth (deg.)	Axial Distance from Core Midplane (mm)	M/C Ratio		
		$^{54}Fe(n,p)^{54}Mn$	$^{58}Ni(n,p)^{58}Co$	$^{93}Nb(n,n')^{93m}Nb$
270.00	1500	0.90	0.87	--
270.00	1200	0.97	0.95	0.83
270.00	900	0.99	0.99	--
270.00	600	0.95	0.97	0.92
270.00	300	1.18	1.17	--
270.00	0	0.88	0.88	--
270.00	-300	0.99	0.91	0.87
270.00	-589	0.79	0.97	1.10
270.00	-900	0.87	0.92	0.98
270.00	-1200	0.90	0.93	--
270.00	-1500	0.90	0.95	--
273.75	0	0.90	0.95	--
277.50	0	0.94	0.98	0.94
281.25	0	0.98	0.99	1.32
285.00	0	1.01	1.08	--
288.75	0	1.16	1.23	1.13
292.50	0	1.12	1.17	--
296.25	0	1.16	1.17	1.45
300.00	0	1.06	1.01	0.94
303.75	0	1.04	1.06	1.19
307.50	0	1.00	1.04	1.22
311.25	0	1.03	1.07	--
315.00	0	1.01	1.03	1.20
315.00	-589	0.99	1.01	1.01
Average		0.99	1.01	1.08
% std dev		10.0	9.5	16.9

Table A-7

Comparison of Average Measured and Calculated Threshold Reaction Rates for Westinghouse 3-Loop Pressure Vessel Clad Samples

Reaction	Average M/C Ratio	% std dev
$^{54}Fe(n,p)^{54}Mn$	0.99	10.0
$^{58}Ni(n,p)^{58}Co$	1.01	9.5
$^{93}Nb(n,n')^{93m}Nb$	1.08	16.9
Linear Average	1.02	12.2

A.5 CONCLUSION

The comparisons described in this appendix have demonstrated methodological equivalence between RAPTOR-M3G and TORT. Further, all comparisons generated using RAPTOR-M3G show good agreement between measurements and calculations. Therefore, RAPTOR-M3G may be used by Westinghouse interchangeably with the TORT code. It may be applied in any situation where a full three-dimensional discrete ordinates flux solution is deemed desirable or necessary.

APPENDIX B EVALUATION OF THE BUGLE-B7 CROSS-SECTION LIBRARY

BUGLE-B7[30] is a revision of the BUGLE-96 cross-section library[11] that incorporates updated cross-section data from the Cross Section Evaluation Working Group (CSEWG).

The Oak Ridge National Laboratory (ORNL) documentation provided with the BUGLE-B7 library includes comprehensive testing of BUGLE-B7 and comparisons between BUGLE-96 and BUGLE-B7 using measured data from the H. B. Robinson-2 and VENUS-3 benchmarks. These tests are sufficient to demonstrate that both the BUGLE-B7 and BUGLE-96 libraries are suitable for light water reactor (LWR) shielding applications that primarily depend on characterizing the fast and epithermal portions of the neutron spectrum. Examples of such applications include determination of fast neutron fluence ($E > 1.0$ MeV) and Iron Atom Displacements (DPA) for reactor material embrittlement calculations and the evaluation of most light water reactor dosimetry.

However, additional testing performed by Westinghouse has revealed differences between radiation transport calculation results generated with the BUGLE-B7 and BUGLE-96 libraries for some applications that were not considered by ORNL. The differences appear to result from discrepancies in the upscatter-removed BUGLE-B7 library for data representing low energy neutrons.

Oak Ridge National Laboratory has been notified of this discrepancy and they are currently investigating the issue. Until the issue is resolved, BUGLE-96 will remain in-use at Westinghouse.